Integrative small and long RNA-omics analysis of human healing and non-healing wounds discovers cooperating microRNAs as therapeutic targets

Zhuang Liu[1,6], Letian Zhang[1,6], Maria A. Toma[1], Dongqing Li[1,2], Xiaowei Bian[1], Irena Pastar[3], Marjana Tomic-Canic[3], Pehr Sommar[4]* and Ning Xu Landén[1,5]*

[1]Dermatology and Venereology Division, Department of Medicine Solna, Center for Molecular Medicine, Karolinska Institutet, 17176 Stockholm, Sweden

[2]Institute of Dermatology, Chinese Academy of Medical Sciences and Peking Union Medical College, Nanjing, Jiangsu, China

[3]Wound Healing and Regenerative Medicine Research Program, Dr Phillip Frost Department of Dermatology and Cutaneous Surgery, University of Miami Miller School of Medicine, Miami, FL, USA.

[4]Department of Plastic and Reconstructive Surgery, Karolinska University Hospital, Stockholm, Sweden

[5]Ming Wai Lau Centre for Reparative Medicine, Stockholm Node, Karolinska Institute, 17177 Stockholm, Sweden

[6]Equal contribution

*Co-senior authors

To whom correspondence should be addressed: Email: ning.xu@ki.se or pehr.sommar@regionstockholm.se

Abstract

MicroRNAs (miR) are important posttranscriptional regulators and exhibit a high potential to be utilized in diagnosis and therapy. However, our insufficient knowledge of the miR-mediated gene regulation in human skin wound healing severely hinders the identification of clinically relevant miRs. Here, we performed paired small RNA and long RNA sequencing in human tissue samples, including matched skin and acute wounds collected at each healing stage and chronic non-healing venous ulcers (VU). With integrative small and long RNA-omics analysis, we developed a compendium (https://www.xulandenlab.com/humanwounds-mirna-mrna), which will be an open, comprehensive resource to broadly aid wound healing research. With this first clinical, wound-centric resource of miRs and mRNAs, we identified 17 pathologically relevant miRs that exhibited abnormal VU expression and displayed their targets enriched explicitly in the VU gene signature. Intermeshing regulatory networks controlled by these miRs revealed their high cooperativity in contributing to chronic wound pathology characterized by persistent inflammation and proliferative phase initiation failure. Furthermore, we demonstrated that miR-34a, miR-424, and miR-516, upregulated in VU, cooperatively suppressed keratinocyte growth while promoting inflammatory response. Collectively, our study opens the possibility of developing innovative wound treatment that targets pathologically relevant cooperating miRs to attain higher therapeutic efficacy and specificity.

Keywords: microRNA, regulatory network, wound healing, chronic wound, venous ulcer

Introduction

Wound healing is a fundamental biological process comprising three sequential and overlapping phases, i.e., inflammation, proliferation, and remodeling(Reinke & Sorg, 2012). This delicate repair process is often disrupted in chronic venous insufficiency patients, resulting in venous ulcers (VU) characterized by persistent inflammation and proliferative phase initiation failure(Eming et al., 2014). VU is the most common chronic non-healing wound type, comprising 45–60% of all lower extremity ulcerations(Vivas et al., 2016). VU exhibits a marked impact on health-related life quality and represents a significant financial burden both to the patients and the society with an annual health care cost of overall $14.9 billion in the USA(Hoversten et al., 2020). A deeper understanding of the underlying gene expression regulatory mechanisms during physiological and pathological wound repair is essential for developing more effective wound treatments(Stone et al., 2017).

MicroRNAs (miR) represent a group of short (~22 nt) non-coding ribonucleic acids, incorporating into the RNA-induced silencing complex and binding to the 3' untranslated region of their target mRNAs, resulting in mRNA destabilization and translational repression(Stavast & Erkeland, 2019). Given that an individual miR can target dozens to hundreds of genes, miRs have been identified as regulators of complex gene networks(Stavast & Erkeland, 2019). MiR-mediated regulation is reportedly crucial in multiple fundamental biological processes including skin wound repair(Herter & Xu Landen, 2017; Meng et al., 2018). Importantly, manipulating miRs critical for the disease pathogenesis could offer a prominent therapeutic effect, supported by viral infection- and cancer-targeting miR therapeutics clinical trials(Rupaimoole & Slack, 2017). Therefore, miR-based therapeutics for hard-to-heal wounds represent a promising approach(Herter & Xu Landen, 2017; Luan et al., 2018; Meng et al., 2018; Nie et al., 2020; Pastar et al., 2021; Sen & Roy, 2012).

However, our insufficient knowledge of the miR-mediated gene regulation in human wounds severely hinders the identification of clinically relevant miRs and their potential therapeutic use. While most previous wound healing-related miR studies rely on *in vitro* or animal models, only a few have approached miR profiles in human wound tissues or primary cells from patients, including tissues and fibroblasts of diabetic foot ulcers(Liang et al., 2016; Ramirez et al., 2018), burn wound dermis(Liang et al., 2012), and acute wounds at the inflammatory phase(Li et al., 2015). Despite sharing several fundamental features, the human skin structure and repair processes are different from those of the commonly used animal models (e.g., rodents)(Elliot et al., 2018). Moreover, animal models cannot fully

simulate the human disease complexity, and the findings are difficult to extrapolate to humans(Darwin & Tomic-Canic, 2018; Pastar et al., 2018). Thereby, a rigorous and in-depth characterization of miR-mediated gene regulatory networks in human healing and non-healing wounds is timely needed.

In this study, we performed paired small and mRNA expression profiling in the human skin, acute wounds during the inflammatory and proliferative phases, and VU, unraveling time-resolved changes of the whole transcriptome throughout the wound healing process and the unique gene expression signature of a common chronic wound type. The integrative miR and mRNA omics analysis provides a network view of miR-mediated gene regulation in human wounds *in vivo* and demonstrates the functional involvement of miRs in human skin wound repair at the system level. Importantly, we identified miRs highly relevant to VU pathology, based not only on their aberrant expression but also their targetome enriched in the VU-related gene expression signature. Apart from confirming the *in silico* findings, the experimental miR expression, targetome, and function validation uncovered that VU-dysregulated miRs could act cooperatively contributing to the stalled wound healing characterized by failed transition from inflammatory-to-proliferative phase, which opens up new possibility for the development of more precise and innovative wound treatment targeting pathologically-relevant cooperating miRs to achieve higher therapeutic efficacy and specificity. Additionally, based on this comprehensive analysis of human wound tissues, we built a browsable resource web portal (https://www.xulandenlab.com/humanwounds-mirna-mrna), which is the first wound healing-focused miR resource for facilitating the exploration of miR's clinical application and for aiding in the elucidation of posttranscriptional regulatory underpinnings of tissue repair.

Materials and Methods

Human wound samples

Human wound biopsies were obtained from 10 healthy donors and 12 patients with chronic venous ulcer (VU) at the Karolinska University Hospital Solna (Stockholm, Sweden). Donor demographics are presented in **Table 1**. Patients with VUs, which persisted for more than four months despite conventional therapy, were enrolled in this study (**Table 2**). Tissue samples were collected from the lower extremity at the nonhealing edges of the ulcers by using a four-mm biopsy punch (**Figure 1a**). Healthy donors above 60 years old without skin diseases, diabetes, unstable heart disease, infections, bleeding disorder, immune suppression, and any ongoing medical treatments were recruited (**Table 3**).

103 Two full-thickness excisional wounds (4 mm in diameter) were created at the lower extremity on each
104 donor, and the excised skin was saved as intact skin control (Skin). The wound-edges were excised
105 with a six mm-biopsy punch at day one (Wound1) and day seven (Wound7) after wounding (**Figure 1a**).
106 Written informed consent was obtained from all the donors to collect and use the tissue samples. The
107 study was approved by the Stockholm Regional Ethics Committee and conducted according to the
108 Declaration of Helsinki's principles.

109 **RNA extraction, library preparation, and sequencing**

110 *RNA extraction* Snap frozen tissue samples were homogenized with the TissueLyser LT (Qiagen), and
111 total RNA was isolated using the miRNeasy Mini kit (Qiagen). RNA quality and quantity were determined
112 by using Agilent 2100 Bioanalyzer (Agilent Technologies) and Nanodrop 1000 (Thermo Fisher Scientific
113 Inc.), respectively.
114
115 *Small RNA library preparation and sequencing* The small RNA sequencing libraries were constructed
116 using 3 µg total RNA per sample and NEB Next® Multiplex Small RNA Library Prep Set for Illumina®
117 (NEB) following the manufacturer's recommendation. Briefly, total RNA was first ligated to adaptors at
118 the 3' end by NEB 3' SR adaptor and 5' end by T4 RNA ligase followed by reverse transcription into
119 cDNA using M-MuLV Reverse Transcriptase. PCR amplification of cDNA was performed using SR
120 primers for Illumina and index primers. The PCR products were purified, and DNA fragments spanning
121 from 140 to 160bp were recovered and quantified by DNA High Sensitivity Chips on the Agilent
122 Bioanalyzer. The libraries were sequenced on an Illumina Hiseq 2500 platform (Illumina, Inc.) using
123 single-end 50bp reads, and all samples were run side by side.
124
125 *mRNA library preparation and sequencing* The long RNA sequencing libraries were constructed with a
126 total amount of 2 µg RNA per sample. First, the ribosomal RNA was depleted by Epicentre Ribo-zero®
127 rRNA Removal Kit (Epicentre). Second, strand-specific total-transcriptome RNA sequencing libraries
128 were prepared by incorporating dUTPs in the second-strand synthesis step with NEB Next® Ultra™
129 Directional RNA Library Prep Kit for Illumina® (NEB). Finally, the libraries were sequenced on an
130 Illumina Hiseq 4000 platform, and 150 bp paired-end reads were generated for the following analysis.

131

132 **Analysis of miRNA-sequencing data**

133 *Quality control, mapping, and quantification* Quality of raw data was assessed using FastQC v0.11.8
134 (http://www.bioinformatics.babraham.ac.uk/projects/fastqc/). We used mapper.pl module in the
135 miRDeep2 v0.1.3 package(Friedlander et al., 2012; Mackowiak, 2011) to filter low-quality reads and
136 remove sequencing adaptors and redundancies. Trimmed reads with lengths greater than 18
137 nucleotides were mapped to GENCODE human reference genome (hg38) by the software Bowtie
138 v1.2.2(Langmead et al., 2009). The miRDeep2.pl module was then performed with default parameters
139 to identify known miRNAs, which were compared to miRNAs in miRBase release 22.1(Kozomara et al.,
140 2018). Counts of reads mapped to each known mature miRNAs were acquired from the quantifier.pl
141 module output without allowing mismatch. miRNAs with read counts less than five in more than half of
142 twenty samples were discarded since these miRNAs are unlikely to give stable and robust results. Raw
143 counts of 562 miRNAs were normalized for sequencing depth using TPM methods (transcript per million
144 = mapped read count/total reads * 10e6)(Zhou et al., 2010) and prepared for further analysis.

145 *Differential expression (DE) analysis* The DESeq2 workflow(Love et al., 2014) was carried out to fit raw
146 counts to the negative binomial (NB) generalized linear model and to calculate the statistical
147 significance of each miRNA in each comparison. In particular, the paired model was employed when
148 comparing samples from the same donor. *P-value*s obtained from the Wald test were corrected using
149 Benjamini-Hochberg (BH) multiple test to estimate the false discovery rate (FDR). The differentially
150 expressed miRNAs were defined as FDR < 0.05 and |log2(fold change)| ≥ 1.

151 *Principal component analysis (PCA)* To explore the similarity of each sample, PCA was performed by
152 using a DESeq2 built-in function *plotPCA* on the transformed data, in which the variances and size
153 factors were stabilized and corrected. PCA and heatmaps were plotted by using *ggplot2*(Hadley, 2016)
154 and *ComplexHeatmap*(Gu et al., 2016) packages in RStudio (https://rstudio.com/).

155 *Weighted gene co-expression network analysis (WGCNA)* The normalized expression of 562 miRNAs
156 were used as input to the WGCNA R package(Langfelder & Horvath, 2008). First, we calculated the
157 strength of pairwise correlations between miRNAs using the 'biweight' mid-correlation method. The
158 function *pickSoftThreshold* was then employed to compute the optimized soft-thresholding power based
159 on connectivity, which led to an approximately scale-free network topology(Zhang & Horvath, 2005).
160 Second, a signed weighted co-expression network was constructed with a power of 18 using the one-

161 step *blockwiseModules* algorithm (**Figure 2 - figure supplement 2a**). Network modules were filtered
162 according to parameters: *minModuleSize* = 10 and *mergeCutHeight* = 0.25.
163 The expression profile of each module was represented by the module eigengene (ME), referred to as
164 the first principal component of all miRNAs in each module. Pearson correlations (values from -1 to 1)
165 and the corresponding *P-value*s between MEs and traits were computed. *P-value*s were further
166 adjusted to FDR across all the modules using the BH method. Modules significantly associated with
167 each trait were selected by FDR < 0.05 and absolute correlation coefficients > 0.4. The module
168 membership (also known as kME) of each miRNA was calculated by the correlations between miRNA
169 expression and ME. MiRNAs with the highest kME values were defined as intra-modular hub miRNAs,
170 and networks of hub miRNAs in significant modules were visualized using the Cytoscape v3.7.2
171 software(Shannon et al., 2003).
172 To check the robustness of module definition, we carried out module preservation analysis and
173 calculated the standardized Z-scores for each module by permutating 200 times using the same 20
174 samples as reference and test datasets. Modular preservation is strong if Z-summary > 10, weak to
175 moderate if 2 < Z-summary < 10, no evidence of preservation if Z-summary ≤ 2(Langfelder et al., 2011).

176 *Transcription factor (TF) enrichment analysis* We leveraged a curated database about TF-miRNA
177 regulations, TransmiR v2.0(Tong et al., 2019), to identify the TFs regulating miRNA expression in each
178 module. Fisher's exact tests were employed to evaluate the enrichment of each TF in the significant
179 modules, and FDRs were adjusted to the total number of TFs (Odds ratio > 1 and FDR < 0.05).
180 Correlations of gene expression between TFs and miRNA modules (represented by MEs) were further
181 filtered to identify putative TF-mediated miRNA gene expression patterns (Pearson correlation: *P-value*
182 < 0.05, coefficient > 0). The 562 miRNAs abundantly expressed in our samples were treated as the
183 background dataset.

184

185 **Analysis of mRNA sequencing data**

186 Raw reads of mRNA sequencing were first trimmed for adaptors and low-quality bases using
187 Trimmomatic v0.36 software(Bolger et al., 2014). Clean reads were aligned to the human reference
188 genome (GRCh38.p12), coupled with the comprehensive gene annotation file (GENCODEv31) using
189 STAR v2.7.1a(Dobin et al., 2013). Gene expression was then quantified by counting unique mapped

190 fragments to exons by using the feature count function from the Subread package(Liao et al., 2013).
191 Raw counts for each gene were normalized to fragments per kilobase of a transcript, per million mapped
192 reads (FPKM)-like values. Only mRNAs with FPKM ≥ 1 in at least ten samples were kept for the rest
193 analysis. We used the same pipeline described above for mRNA DE and PCA analysis. The
194 differentially expressed mRNAs were defined as FDR < 0.05 and |log2(fold change)| ≥ 0.58. WGCNA
195 was carried out for 12,069 mRNAs with the optimal threshold power of 12 according to a fit to the scale-
196 free topology of the co-expression network (**Figure 2 - figure supplement 4a**). Thirteen mRNA
197 modules were identified with the settings: *maxBlockSize* = 20000, *minModuleSize* = 100 and
198 *mergeCutHeight* = 0.25. Furthermore, mRNA module-enriched TF analysis was performed with a
199 manually curated TF-target regulatory relationship database, TRRUST v2(Han et al., 2018), using
200 Fisher's exact tests. TFs with FDR < 0.05 and odds ratio > 1 and the expression significantly correlated
201 with respective mRNA modules (Pearson correlation *P-value* < 0.05) were identified.

202 *Gene ontology (GO) analysis* We carried out GO analysis for mRNAs by using the WebGestalt tool
203 (http://www.webgestalt.org/)(Liao et al., 2019), which applied a hypergeometric test in target and
204 reference gene sets. GO terms of non-redundant biological process (BP) with gene number less than
205 10 and adjust *P- value* (FDR) > 0.05 were filtered out.
206

207 **Integrative analysis of miRNA and mRNA expression changes in wound healing**

208 *Expression correlation between mRNA and miRNA modules* An integrative analysis was carried out by
209 relating the first principal component (PC1) of miRNA expression, calculated using the
210 *moduleEigengenes* function of WGCNA package(Langfelder & Horvath, 2008), to the PC1 of mRNA
211 expression in each module. The miRNA-mRNA module pairs with a Pearson correlation coefficient < -
212 0.5 and a *P-value* < 0.05 were selected for the following enrichment analysis.

213 *Prediction of miRNA targets* We predicted both conserved and non-conserved target sites for all the
214 562 miRNAs by using the *get_multimir* function from R package multimiR(Ru et al., 2014)
215 (http://multimir.org/) based on the latest TargetScan v7.2 database(Agarwal et al., 2015; Lewis et al.,
216 2005). All predicted miRNA targets were sorted by a primary score calculated for target site strength,

217 and the top 25% with summed context++ score ≤ -0.15 were defined as the strongest miRNA targets.
218 Targets that were not detected by the long RNA-seq were removed.

219 *Gene set enrichment analysis of miRNA targets in mRNA modules.* We evaluated the degree of
220 enrichment of miRNA modules' targets in mRNA modules. For this, we focused on the VU-specific DE
221 miRNA, i.e., the 22 up- and 10 down-regulated miRNAs in VU compared to both the skin and acute
222 wounds (FDR < 0.05 and |log2(fold change)| ≥ 1), as well as the VU-associated modules' hub miRNAs,
223 which kME values were greater than the median kME in respective modules (i.e., 14 miRNAs in m8, 9
224 miRNAs in m12, 20 miRNAs in m7, 29 miRNAs in m3, and 13 miRNAs in m9). Among these miRNAs'
225 strongest targets, we selected the ones that were hit by ≥ 2 miRNAs from m8, m9, m12 modules or
226 miRNAs downregulated in VU; ≥ 3 miRNAs from m7 module or miRNAs upregulated in VU; ≥ 4 miRNAs
227 from m3 module, to capture putative module-driving targets. We performed gene set enrichment
228 analyses for these miRs' targets in VU-specific DE mRNAs (FDR < 0.05 and fold change ≥ 1.5) and
229 VU-associated mRNA modules by using the R function *fisher.test()* based on the two-side Fisher's exact
230 test(Wu et al., 2016). Furthermore, we performed enrichment analysis to identify individual miRNA with
231 their strongest targets significantly enriched in VU-specific DE mRNAs or VU-associated mRNA
232 modules (Fisher's exact test: odds ratio > 1, *P-value* < 0.05).
233

234 **Experimental validation of miRs' expression, targetome, and functions**

235 *Quantitative RT-PCR* To detect miRNA, RNA from human skin and wounds was reverse transcribed
236 using TaqMan® Advanced miRNA cDNA Synthesis Kit (Thermo Fisher Scientific). Individual miRNA
237 expression was then quantified using TaqMan® Advanced miRNA Assays (Thermo Fisher Scientific)
238 and normalized with miR-361-5p and miR-423-5p due to their relatively constant expression between
239 human skin and wounds. To detect mRNA, we performed reverse transcription using the RevertAid
240 First Strand cDNA Synthesis Kit (ThermoFisher Scientific). Gene expression was examined by SYBR
241 Green expression assays (ThermoFisher Scientific) and normalized with housekeeping gene B2M and
242 GAPDH. The primer sequences for B2M are forward primer (5'-AAGTGGGATCGAGACATGTAAG-3')
243 and reverse primer (5'-GGAGACAGCACTCAAAGTAGAA-3'); GAPDH forward primer (5'-
244 GGTGTGAACCATGAGAAGTATGA-3') and reverse primer (5'-GAGTCCTTCCACGATACCAAAG-3').

245 *Primary cell culture and transfection* Adult human epidermal keratinocytes were cultured in EpiLife
246 serum-free keratinocyte growth medium supplemented with Human Keratinocyte Growth Supplement
247 (HKGS) and 100 units/mL Penicillin and 100 µg/mL Streptomycin (Thermo Fisher Scientific). Adult
248 human dermal fibroblasts were cultured in Medium 106 supplemented with Low Serum Growth
249 Supplement (LSGS) and 100 units/mL Penicillin and 100 µg/mL Streptomycin (Thermo Fisher Scientific).
250 Cells were incubated at 37°C in 5% CO_2, and media was routinely changed every 2–3 days. Third
251 passage keratinocytes at 50%-60% confluence were transfected with 20 nM miRNA mimics (Horizon)
252 or negative control using Lipofectamine™ 3000 (Thermo Fisher Scientific).

253 *Microarray analysis* Transcriptome profiling of keratinocytes and fibroblasts transfected with 20 nM
254 miRNA mimics or control mimics for 24 hours (in triplicates) was performed using Affymetrix Genechip
255 system at the Microarray Core facility of Karolinska Institute. Normalized expression data (log2
256 transformed value) were exported from Transcriptome Analysis Console (TAC) software and analyzed
257 by the *limma* R package(Ritchie et al., 2015). In brief, expression data were first fitted to a linear model
258 for each probe. Then, the empirical Bayes method was applied to compute the estimated coefficients
259 of gene-wise variability and standard errors for comparisons of experimental and control groups. Genes
260 with FC > 1.2 and *P*-value < 0.05 between the miRNA mimics- and the control mimics-transfected cells
261 were considered to be significantly changed. Gene set enrichment analysis, including biological process
262 (BP), Kyoto Encyclopedia of Genes and Genomes (KEGG) pathway, and hallmark from Molecular
263 Signatures Database (MSigDB) (http://www.gsea-msigdb.org/)(Subramanian et al., 2005), was
264 performed with a ranked fold change list of all the genes by using the *fgsea* R package(Korotkevich et
265 al., 2021) and visualized by using the *ggplot2*(Hadley, 2016) and *circlize*(Gu et al., 2014) packages.

266 *Immunofluorescence staining* Cells transfected with a combination of miRNA and/or control mimics (50
267 nM in total) were fixed in 4% paraformaldehyde (PFA) for 15 minutes. Cells were incubated with the Ki-
268 67 antibody (Cell Signaling Technology) overnight at 4°C. The next day, cells were incubated with the
269 secondary antibody conjugated with Alexa 488 for 40 minutes at room temperature. Cells were mounted
270 with the ProLong™ Diamond Antifade Mountant with 4',6-Diamidino-2-Phenylindole (DAPI)
271 (ThermoFisher Scientific). Ki-67 signals were visualized with Nikon microscopy, and positive cells were
272 counted using ImageJ software (National Institutes of Health).

273 *Cell proliferation assay* Cells were seeded in 12-well plates with a density of 20,000 cells/well. The
274 plates were placed in IncuCyte live-cell imaging and analysis platform (Essen Bioscience) after cells

275 attaching to the plates. Plates were imaged every two hours, and pictures were processed and analyzed
276 using IncuCyte ZOOM 2018A software (Essen Bioscience).

277 *Statistical analysis* Sample size of each experiment is indicated in the figure legend. Data analysis was
278 performed by using R and Graphpad Prism 7 software. Comparison between two groups was performed
279 with Mann-Whitney U tests (unpaired, non-parametric), Wilcoxon signed-rank test (paired, non-
280 parametric), or two-tailed Student's t-test (parametric). The cell growth assay was analyzed by using
281 two-way ANOVA. P-value < 0.05 is considered to be statistically significant.

282

283 **Results**

284 **miRNA and mRNA paired expression profiling in human wounds**

285 To better understand tissue repair in humans, we collected wound-edge tissues from human acute
286 wounds and chronic non-healing VUs (**Figure 1a** and **Table 1–3**). We created 4mm full thickness punch
287 wounds at the lower legs of healthy volunteers aged beyond 60 years to match the advanced age of
288 VU patients and anatomical location of the highest VUs occurrence(Vivas et al., 2016). Tissue was
289 collected at baseline (Skin), and at day one and day seven post-wounding (Wound1 and Wound7) to
290 capture the inflammatory and proliferative phases of wound healing, respectively. In total, 20 samples
291 divided into four groups, i.e., Skin, Wound1, Wound7, and VU, were analyzed by Illumina small RNA
292 sequencing (sRNA-seq) and ribosomal RNA-depleted long RNA sequencing (RNA-seq). After stringent
293 raw sequencing data quality control (**Table S1** and **S2**), we detected 562 mature miRs and
294 12,069 mRNAs in our samples. Our principal component analysis showed that either the miR or the
295 mRNA expression profiles clearly separated these four sample groups (**Figure 1b**). Next, we performed
296 pairwise comparisons to identify the differentially expressed genes (DEG) during wound repair. We
297 compared the VUs with both the skin and acute wounds and unraveled a VU-specific gene signature,
298 including aberrant increase of 22 miRs and 221 mRNAs and decrease of 10 miRs and 203 mRNAs (DE
299 analysis FDR < 0.05, fold change ≥ 2 for miRs and ≥ 1.5 for mRNAs, **Figure 1c–e** and **Additional file**
300 **1**). The full DEG list can be browsed on our resource website
301 (https://www.xulandenlab.com/humanwounds-mirna-mrna) with more or less rigorous cut-offs. With this
302 unique resource, we dissected further the miR-mediated posttranscriptional regulatory underpinnings
303 of wound repair.

304

305 **Dynamically changed miR expression during wound repair**

306 We leveraged weighted gene co-expression network analysis (WGCNA) for classifying miRs according
307 to their co-expression patterns in the 20 sRNA-seq-analyzed samples to link the miR expression
308 changes with wound healing progression or non-healing status at a system level(Langfelder & Horvath,
309 2008). We identified 13 distinct modules with a robustness confirmed by the module preservation
310 analysis (**Figure 2 - figure supplement 1a**), ten of them significantly correlating (Pearson's correlation,
311 FDR < 0.05) with at least one of the four phenotypic traits, i.e., Skin, Wound1, Wound7, and VU

312 (**Fig. 2a** and **b, Additional file 2**). The WGCNA revealed that module (m)2, m10, and m11 miRs were
313 upregulated at the inflammatory phase (Wound1), while m5 and m6 miRs peaked at the proliferative
314 phase (Wound7). In VU, we identified three downregulated (m3, m7, and m9) and two upregulated (m8
315 and m12) miR modules. We highlighted the 198 "driver" miRs (i.e, the top 20 miRNAs with the highest
316 kME values in each module and kME > 0.5) of the ten significant modules in the co-expression networks
317 (**Figure. 2c, d** and **Figure 2 - figure supplement 2b–i**) and they could also be browsed on our resource
318 web portal (https://www.xulandenlab.com/humanwounds-mirna-mrna). Notably, we identified 84% of
319 them as DEGs, suggesting a high consistence between the WGCNA and DE analysis (**Additional file**
320 **3**).
321
322 We hypothesized that the co-expression of various miRs could be due to their transcription driven by
323 common transcription factors (TF). To test this idea, we leveraged TransmiR v2.0(Tong et al., 2019), a
324 database including literature-curated and ChIP-seq-derived TF-miR regulation data, to identify the
325 enriched TFs in each miR module [Fisher's extract test: odds ratio (OR) > 1, *FDR* < 0.05, **Additional**
326 **file 4**]. Interestingly, the BMP4, KLF4, KLF5, GATA3, GRHL2, and TP53 families exhibited not only
327 their binding sites enriched in the m9 miR genes but their expression also significantly correlated with
328 the m9 miRs (Pearson's correlation coefficient = 0.53–0.82, *P*-value of *p* = 7.05e-06–0.014) (**Figure 2d,**
329 **Figure 2 - figure supplement 3a** and **Additional file 4**). Notably, the BMP4, GATA3, and KLF4
330 expressions were significantly reduced in VU compared to the skin and acute wounds. This result could
331 explain the deficiency of their regulated miRs in VU and also suggest a link between these TFs and
332 chronic wound pathology (**Figure 2 - figure supplement 3b**).
333
334 **mRNA co-expression networks underpinning wound repair**
335 miRs exert functions through the posttranscriptional regulation of their target mRNAs. Therefore,
336 describing the mRNA expression context would be required for understanding the role of miRs in wound
337 repair(Agarwal et al., 2015). We thus performed WGCNA in the paired long RNA-seq data and identified
338 13 mRNA co-expression modules (**Figure. 2e**, **Figure 2 - figure supplement 1b**, **Figure 2 - figure**
339 **supplement 4a–c**, and **Additional file 5**). The GO analysis of the mRNA modules largely confirmed
340 the previous knowledge of wound biology, such as skin hemostasis (M2) and barrier function (M4)-
341 related gene downregulation in the wounds, the upregulation of the genes involved in the immune

342 response (M8), RNA processing, and protein production (M1, M3, and M5) in the inflammatory phase,
343 and the prominent cell mitosis-related gene expression (M7) in the proliferative phase of wound repair
344 (**Figure. 2f** and **Figure 2 - figure supplement 5a**). These results further supported the robustness and
345 reproducibility of our profiling data. Moreover, this unique dataset allows the identification of the key
346 TFs driving these biological processes. For example, we identified NFKB1 and RELA, well-known for
347 their immune functions(Liu et al., 2017), as the most enriched upstream regulators for the M1 mRNAs,
348 while E2F1, a TF promoting cell growth(Ertosun et al., 2016), surfaced as a master regulator TF in M7
349 (**Additional file 6**).
350
351 Importantly, our study unraveled a VU molecular signature: downregulated expression of RNA and
352 protein production- (M1, M3, and M5) as well as cell mitosis-related (M7) genes, and upregulated
353 expression of genes involved in extracellular matrix organization and cell adhesion (M9). These results
354 were in line with the dermal tissue fibrosis observed in patients with chronic venous
355 insufficiency(Blumberg et al., 2012; Pappas et al., 1999; Stone et al., 2020). Moreover, we found an
356 immune gene signature clearly distinguishing the chronic inflammation in VUs (M11 and M12 enriched
357 with adaptive immunity-related mRNAs) from the self-limiting immune response in acute wounds (M8
358 enriched with neutrophil activation- and phagocytosis-related mRNAs) (**Figure 2f** and **Figure 2 - figure**
359 **supplement 5b**). Overall, we generated a gene expression map of human healing and non-healing
360 wounds, setting a stepping stone for the in-depth understanding of the VU pathological mechanisms.
361 After having established this map, we decided to dissect how miRs contribute to these pathological
362 changes.
363
364 **Integrative analysis of miR and mRNA expression changes in wound healing**
365 Among the multiple gene expression regulatory mechanisms, we aimed to evaluate how miRs could
366 contribute to the protein-coding gene expression in human wound repair. We thus performed a
367 correlation analysis for the miRs and mRNAs that were differentially expressed in VU compared to the
368 skin and acute wounds, using the first principal component (PC1) of their expression in each sample.
369 We found significantly negative correlations (Pearson's correlation, P-values: 1.36e-12–1.27e-04)
370 between the PC1 of the DE miRs and the DE mRNAs predicted as miR targets, indicating negative
371 regulation of VU-mRNA signature by the aberrantly expressed miRs in VU (**Figure 3a–c**).

372 Furthermore, we dissected the potential regulatory relationship between the VU-associated miR and
373 mRNA modules. We identified significantly negative correlations between the downregulated miR (m3,
374 m7, and m9) and the upregulated mRNA (M9, M11, and M12) modules, as well as between the
375 upregulated miR (m8 and m12) and the downregulated mRNA (M5) modules in VU (**Figure 3d**). Among
376 these miR-mRNA module pairs, we found that the predicted targets of the downregulated m9 miRs
377 were significantly enriched (Fisher's extract test: OR > 1, *P*-value < 0.05) for the upregulated M9
378 mRNAs, whereas the targets of the upregulated miRs and m8 miRs were enriched for the
379 downregulated mRNAs and M5 mRNAs (**Figure 4a** and **Additional file 7**). These results demonstrated
380 that miRs significantly contribute to the aberrant mRNA expression in VU at a global level.
381 Based on the above-identified miR-mRNA module pairs, we next searched for individual candidate miRs
382 with their targets enriched for the VU mRNA signature. We observed that the targets of two VU-
383 associated downregulated miRs (miR-144-3p and miR-218-5p) and five m9 miRs (miR-205-5p, miR-
384 211-5p, miR-506-3p, miR-509-3p, and miR-96-5p) were enriched for the upregulated M9 mRNAs,
385 whereas the targets of three VU-associated upregulated miRs (miR-450-5p, miR-512-3p, and miR-
386 516b-5p) and seven m8 miRs (miR-424-5p, miR-34a-5p, miR-34c-5p, miR-516a-5p, miR-517a-3p, miR-
387 517b-3p, and miR-7704) were enriched for M5 mRNAs and downregulated mRNAs (**Figure 4b** and
388 **Additional file 8**). These miR targetomes were enriched for the mRNAs associated with VU pathology.
389 Therefore, these miR candidates are of importance for understanding the pathological mechanisms
390 hindering wound healing. Moreover, we compiled miR-mediated gene expression regulation networks
391 centered with these highly pathologically relevant miRs (**Figure 4c**, **Figure 4 – figure supplement 1**,
392 **2** and **Additional file 8**). These networks also include the mRNAs predicted as the strongest targets
393 and with anti-correlated expression patterns with these miRs in human wounds *in vivo*, as well as the
394 TFs reported to regulate these miR expressions from the TransmiR v2 database(Tong et al., 2019).
395 Taken together, our study identifies a list of highly pathological relevant miRs and their targetomes in
396 human VU.
397

398 **Experimental validation of miR expressions and targets in human skin wounds**

399 We selected nine shortlisted DE miRs (**Figure 1d** and **4b**), including three downregulated (miR-149-5p,
400 miR-218-5p, and miR-96-5p) and six upregulated (miR-7704, miR-424-5p, miR-31-3p, miR-450-5p,
401 miR-516b-5p, and miR-517b-3p) miRs in VU, and validated their expression by qRT-PCR in a cohort

402 with seven healthy donors and twelve VU patients, matched in terms of age and the anatomical wound
403 locations (**Table 2** and **3**). We confirmed their expression patterns in RNA-seq, supporting the
404 robustness and reproducibility of our profiling data (**Figure 5a–i**, **Figure 5 – figure supplement 1 and**
405 **Additional file 9**).

406 Furthermore, we experimentally validated the targets of eight miRs surfaced in our analysis (**Figure 4b**),
407 including the miRs downregulated (miR-218-5p and miR-96-5p) and upregulated (miR-424-5p, miR-
408 450-5p, miR-516b-5p, miR-34a-5p, miR-34c-5p, and miR-7704) in VU. We performed genome-wide
409 microarray analysis in human primary keratinocytes or fibroblasts overexpressing each of these miRs.
410 Furthermore, we re-analyzed our published microarray dataset on keratinocytes with miR-34a-5p or
411 miR-34c-5p overexpression (GSE117506)(Pachera et al., 2020). For all these eight miRs, we observed
412 that their strongest targets predicted by TargetScan were significantly downregulated compared to the
413 non-targeting mRNAs (Wilcoxon t-test P-values: 1.34e-25~1.91e-59). The differences were more
414 significant when we divided the strongest targets into conserved and experimentally validated subtypes,
415 confirming the bioinformatics prediction robustness of the miR targets applied in this study (**Figure 5j–**
416 **m** and **Figure 5 – figure supplement 2a - j**).

417 Notably, we observed significant enrichment (Fisher's exact test, OR > 1, *P*-value < 0.05) of the
418 experimentally validated miR-218-5p, miR-34a-5p, miR-34c-5p, and miR-7704 targets for the VU gene
419 signature (**Figure 5n** and **Additional file 9**). We have previously shown that miR-34a and miR-34c
420 inhibit keratinocyte proliferation and migration, while promoting apoptosis and inflammatory response,
421 resulting in delayed wound repair in a mouse model(Pachera et al., 2020). We validated robustness of
422 the bioinformatics approach applied in this study by miR-34a/c re-identification. Here, we discovered
423 that both the predicted (**Figure 4b**) and validated (**Figure 5n**) miR-34a/c targets were enriched for the
424 downregulated M5 module mRNAs in VU. Notably, our microarray analysis confirmed that miR-34a/c
425 reduced the expression of 39 hub genes in the M5 module [log2(fold change) ≤ -0.58, *P*-value < 0.05,
426 Fig. S9j], and 26 of them exhibited negative correlation (Pearson's $r = -0.83 – -0.45$, *P*-value < 0.05)
427 with miR-34a/c expression levels in the human skin and wound samples (**Figure 5o** and **Additional**
428 **file 9**), suggesting that they were miR-34a/c targets *in vivo*. MiR-218-5p was downregulated in the VU
429 compared to the acute wounds and the skin (**Figure 5b** and **Figure 5 – figure supplement 1**). Its
430 predicted (**Figure 4b**) and validated (**Figure 5n**) targets were both enriched for the upregulated or M9
431 module mRNAs in VU. Among the ten *in vitro* validated targets, eight negatively correlated (Pearson's

432 $r = -0.82 \sim -0.46$, *P*-value of $p < 0.05$) with miR-218-5p expression in the human skin and wounds
433 (**Figure 5o**, **Figure 5 – figure supplement 2j**, and **Additional file 9**). Interestingly, this study also
434 identified miR-7704, a human-specific miR, with significantly increased expression in VU (**Figure 5d**
435 and **Figure 5 – figure supplement 1**). Similar to miR-34a/c, the predicted (**Figure 4b**) and validated
436 (**Figure 5n**) miR-7704 targets were highly enriched for the M5 module mRNAs downregulated in VU.

437 For miR-96-5p, miR-424-5p, miR-450-5p, and miR-516b-5p, although their predicted targets were
438 significantly enriched (Fisher's exact test: OR > 1, *P*-value < 0.05) for VU-associated mRNAs
439 (**Figure 4b**), we did not find similar enrichment for their experimentally validated targets. Nevertheless,
440 these miRs regulated some VU-associated hub genes *in vitro* (**Figure 5 – figure supplement 2k**) and
441 also exhibited an anti-correlated expression pattern with their targets *in vivo* (**Figure 5p**), e.g., miR-96-
442 5p from the downregulated m9 module targets the M9 mRNAs upregulated in VU, including TP53INP1,
443 LAMC1, EDNRA, GJC1, and FN1; while miR-424-5p from the upregulated m8 miR module targets the
444 M5 mRNAs downregulated in VU, including SLC25A22, VPS4A, and GHR (**Additional file 9**).

445 In summary, we experimentally validated the expression and targets of the miRs identified by the RNA-
446 seq data bioinformatics analysis, confirming the robustness and reproducibility of this dataset and
447 highlighting its value as a reference for studying the physiological and pathological roles of miRs in
448 human skin wound healing.

449

450 **Cooperativity of VU pathology-relevant miRs**

451 From the miR-mediated gene expression regulation networks underpinning VU pathology (**Figure 4 –**
452 **figure supplement 1, 2,** and **Additional file 8**), we caught a glimpse of presumable miR cooperativity
453 through targeting the same mRNAs, i.e., co-targeting among miRs, which reportedly imposing stronger
454 and more complex repression patterns on target mRNA expression(Cherone et al., 2019). For the miRs
455 with unrelated seed sequences, we found that miR-34a/c and miR-424-5p or miR-7704 shared eight–
456 ten targets, and these miRs were co-expressed in the m8 module. We showed that among the
457 downregulated miRs in VU, miR-96-5p and miR-218-5p shared eight targets.

458 In addition, we performed functional annotations for the genes regulated by the VU-associated miRs
459 identified in the microarray analysis (**Figure 6a** and **Additional file 10**). Both miR-218-5p and miR-96-
460 5p promoted ribosome biogenesis and non-coding (nc) RNA processing, while miR-218-5p also

461 suppressed keratinization. miR-34a/c-5p enhanced innate immune response, while reducing mitosis.
462 Similarly, miR-424-5p and miR-516b-5p increased the cellular defense response, while inhibiting cell
463 proliferation. In addition, we showed that miR-450-5p upregulated genes related to the ncRNA
464 metabolic process and mitochondrial respiratory chain complex assembly, whereas miR-7704
465 downregulated insulin, ERBB, and small GTPase-mediated signaling pathway-related genes. Of
466 particular interest, combining the miR expression changes with their annotated functions, we found a
467 regular pattern, i.e., the miRs upregulated in VU (i.e., miR-34a-5p, miR-34c-5p, miR-424-5p, miR-450-
468 5p, miR-7704, and miR-516-5p) promoted inflammation but inhibited proliferation; whereas the miRs
469 downregulated in VU (i.e., miR-218-5p and miR-96-5p) were required for cell growth and activation
470 (**Figure 6b**). Therefore, these VU-dysregulated miRs might cooperatively contribute to the stalled
471 wound healing characterized with failed transition from inflammation-to-proliferation(Landen et al.,
472 2016).
473
474 **Cooperation of miR-34a, miR-424, and miR-516 in regulating keratinocyte proliferation and**
475 **inflammatory response**
476 To validate miR cooperativity in modulating the key pathological processes in VU, we analyzed
477 proliferation and inflammatory response of keratinocytes overexpressing individual miR or miR
478 combinations. The microarray data gene ontology analysis (**Figure 6b**) showed that three miRs
479 upregulated in VU could suppress the expression of mitotic spindle-related genes (**Figure 6c**): miR-
480 34a/c-5p reduced the level of 41 mRNAs (including two miR-34a/c targets), while miR-424-5p
481 downregulated the expression of 67 mRNAs (including 14 miR-424 targets). Although 33 mRNAs were
482 commonly regulated by miR-34a/c-5p and miR-424-5p, none of them were co-targeted by these miRs
483 (**Figure 6c**). Similarly, in the cell cycle pathway, miR-34a-5p directly targeted CCND1, CDK6, HDAC1,
484 and E2F3, while miR-424-5p targeted ANAPC13, CCNE1, CDC25B, CDK1, CDKN1B, CHK1, WEE1,
485 and YWHAH, and only CDC23 was co-targeted by both miRs (**Figure 7a**). We thus hypothesized that
486 miR-34a-5p and miR-424-5p might cooperate to impact stronger on cell proliferation by targeting
487 different gene sets within the same signaling pathway. To test this idea, we measured keratinocyte
488 growth by detecting proliferation marker gene Ki67 expression both on mRNA and protein levels. We
489 found that although miR-34a-5p or miR-424-5p alone could reduce Ki67 levels, their combination
490 suppressed stronger Ki67 expression (**Figure 7b–c**, **Figure 7 – supplement 1a** and **additional file**

491 **11**). The cooperativity between miR-34a-5p and miR-424-5p in repressing keratinocyte growth was
492 further confirmed by comparing cell growth curves generated with a live cell imaging system (**Figure 7d**,
493 **Figure 7 – supplement 1b** and **Video 1**). Moreover, our microarray analysis showed that the miR-34a-
494 5p and miR-516b-5p combination extended the list of inflammatory response-related upregulated genes
495 (**Figure 6d**). In line with this, simultaneously overexpressing miR-34a-5p and miR-516b-5p induced a
496 higher inflammatory chemokine CCL20 expression compared to the individual overexpression of each
497 miRNA (**Figure 7e**). In summary, our study identified VU signature miRs, e.g., miR-34a, miR-424, and
498 miR-516, with cooperativity in inflicting more severe pathological changes (**Figure 7f**). These findings
499 open new opportunities of developing wound treatment targeting cooperating miRs with potentially
500 higher therapeutic efficacy and specificity.

501 **Discussion**

502 Our genome-wide paired analysis of miR and mRNA expression in human healing and non-healing
503 wounds provides a novel global landscape of the miR regulatory roles in wound biology. A detailed
504 overview of the mRNA expression context at different healing stages or under pathological condition
505 VU allows a more precise understanding about the complex role of miRs in wound repair. The same
506 miR is often described to play different or even opposite roles in different cells, as each cell type has
507 specific gene expression context subjected to the miR-mediated posttranscriptional regulation(Erhard
508 et al., 2014). Thereby, the different mRNA expression profiles in acute or chronic wounds should be
509 considered to understand the precise role of an miR in these distinct contexts. With this aspect in mind,
510 we highlight miRs with their targetome most enriched in the VU mRNA signature, as these miRs display
511 a higher likelihood to regulate pathologically relevant genes. Notably, certain of these miRs did not
512 exhibit the greatest expression change in VU, they would thus be missed with the commonly used
513 strategy that focuses on the top miR expression profiling data changes.

514 Another strength of our study is the decryption of time-resolved miR-mRNA expression pattern during
515 human skin wound healing, providing a temporal view to our understanding of the functional miR roles.
516 miRs and their target gene expression contexts change dynamically to support different functional
517 needs during wound repair. Defining an miR as “pro-healing” or “anti-healing” requires specifying its
518 temporal expression pattern. For example, continuous expression of a miR that is beneficial for one
519 healing phase but not the other might also lead to deleterious effects.

520 To understand the molecular mechanisms underlying the miR co-expression patterns, we analyzed the
521 enriched TFs for each miR module with experimentally validated TF-miR regulation data(Tong et al.,
522 2019). This analysis led us to important TFs, such as BMP4(Botchkarev, 2003; Lewis et al., 2014) and
523 GATA3(Kaufman et al., 2003; Kurek et al., 2007) that play fundamental roles in skin development and
524 postnatal remodeling, as well as KLF4, crucial for establishing skin barrier function(Segre et al., 1999).
525 Notably, both GATA3 and KLF4 are reportedly downregulated in human VU(Stojadinovic et al., 2014;
526 Stojadinovic et al., 2008). Our study confirms these findings and provides a novel insight, showing that
527 the loss of these TFs might contribute to VU pathology through their regulated miRs.

528 Numerous miRs that reportedly regulate wound healing in animal models also surfaced in our study,
529 supporting the robustness of our profiling data and bioinformatics analysis. Thereby, our data would be

530 potentially helpful to evaluate the clinical relevance of these miRs. For example, miR-34a/c reportedly
531 enhance keratinocyte inflammatory response, while suppressing proliferation and migration in cultured
532 cells and mouse wound models(Wu et al., 2020). miR-34a was also identified as one of the most
533 induced miRs in diabetic foot ulcer fibroblasts. Induction of miR-34a together with miR-21-5p and miR-
534 145-5p inhibits fibroblast movement and proliferation, whereas activates cell differentiation and
535 senescence(Liang et al., 2016). In this study, we described that miR-34a/c were specifically upregulated
536 in VU, whereas their levels during wound repair remained relatively low and stable, suggesting their
537 specific role in wound pathology. miR-34 targets were enriched in the M5 mRNA module, containing
538 genes upregulated in the inflammatory phase of wound healing but downregulated in VUs. The VU-
539 relevant miR-34 targetome identified in this study would be potentially useful for determining the precise
540 role of miR-34 in VU pathology. Our current findings in human samples together with previous functional
541 data(Liang et al., 2016; Wu et al., 2020) suggest that miR-34 inhibition along with modulation of
542 additional deregulated miRs might be a promising VU treatment approach.

543 In addition, certain of these VU-related miRs are involved in skin-related functions but have not yet been
544 linked to wound healing. For example, miR-218-5p regulates hair follicle development(Zhao et al., 2019),
545 inhibits melanogenesis(J. Guo et al., 2014), and enhances fibroblast differentiation(F. Guo et al., 2014).
546 miR-7704 was identified as an exosomal miR produced by melanocytes(Shen et al., 2020). miR-424-
547 5p suppresses keratinocyte proliferation(Ichihara et al., 2011) and cutaneous angiogenesis(Nakashima
548 et al., 2010; Yang et al., 2017). Moreover, our VU-related miR list (**Figure 4b**) also contains miRs
549 without prior knowledge in their role either in skin or wound healing, e.g., miR-517a-3p, miR-517b-3p,
550 miR-516b-5p, miR-512-3p, and miR-450-5p. It would be highly interesting to examine the role of these
551 miRs in VU. Overall, our dataset can serve as a valuable reference for prioritizing clinically relevant
552 miRs for further functional studies.

553 Moreover, we studied the relationships between the dysregulated miRs in VU, regarding their target
554 repertoire and biological functions and identified miRs that could act cooperatively. Such knowledge is
555 required for developing combined miR therapeutics with increased specificity and efficacy(Lai et al.,
556 2019). In the miR-target networks underpinning VU (**Figure 4 – figure supplement 1** and **2**), we
557 identified a few putative cooperating miR pairs/clusters that were co-expressed and shared multiple
558 common targets, including the upregulated miR-34a/c together with miR-424-5p and miR-7704, as well
559 as the downregulated miR-218-5p and miR-96-5p in VU. Furthermore, although not sharing targets, the

560 majority of the VU-dysregulated miRs could still regulate the common biological processes coordinately.
561 For example, the miRs upregulated in VU (e.g., miR-34a/c-5p, miR-424-5p, miR-450-5p, miR-7704,
562 and miR-516-5p) promote inflammation but inhibit proliferation; whereas the miRs downregulated in VU
563 (e.g., miR-218-5p and miR-96-5p) are needed for cell growth and activation. As a combined
564 consequence, this VU-miR signature could disrupt the swift transition from inflammation to proliferation
565 (**Figure 7f**). The failure of this phase transition represents a core pathology of chronic wounds(Eming
566 et al., 2014; Landen et al., 2016). Our findings open the possibility of developing innovative wound
567 treatment targeting multiple pathologically relevant cooperating miRs to attain higher therapeutic
568 efficacy and specificity.

569 Based on the integrative small and long RNA-omics analysis of human wound tissues, we have
570 developed an openly available compendium (https://www.xulandenlab.com/humanwounds-mirna-mrna)
571 for the research community. This novel, rich resource enabled us to gain a network view of miR-
572 mediated gene regulation during human physiological and pathological wound repair in vivo. With the
573 same sequencing datasets, we have also analyzed circular RNA expression and their potential
574 interaction with miRs and miR targets(Toma et al., 2021), which results can be queried at
575 https://www.xulandenlab.com/humanwounds-circrna. These efforts result in many testable hypotheses
576 for future studies elucidating gene expression regulatory mechanisms underpinning tissue repair.

577 A limitation of our study is the lack of cell type specific miR expression data. Certain gene expression
578 changes detected in the tissue biopsies might be due to the changes of cellular compositions. To rule
579 out this possibility, we validated miR-mediated gene regulation in individual skin cell types (i.e.,
580 keratinocytes and fibroblasts) for several miRs surfaced in our analysis. However, to systemically
581 differentiate the gene expression regulation occurring in an individual cell from the altered cellular
582 composition in wound tissues requires future studies using single-cell small RNA sequencing, which
583 technology still remains challenging to be used at a scale for analyzing complex dynamics of tissue,
584 such as human skin and wounds, as it needs extensive cell handing and therefore has only been applied
585 to few cells(Nielsen & Pedersen, 2020). As new technologies for higher cellular resolution miRNA
586 analyses emerge, we hope that such approach will be feasible in a near future.

587

588 **Conclusion**

589 In conclusion, this genome-wide, integrative analysis of miR and mRNA expression in human skin and
590 wound tissues reinforce and extend the evidence about the functional role of miRs in wound repair and
591 their therapeutic potential for chronic wound treatment. By combining miR expression patterns with their
592 specific target gene expression context, we identified miRs highly relevant to VU pathology. This
593 rigorous and in-depth molecular characterization of human wound tissues adds a novel dimension to
594 our current knowledge mostly relying on non-human models and would serve as a unique platform and
595 valuable resource for further mechanistic studies of miRs with a high translational potential.

596 **Data availability**

597 Raw data of small RNA sequencing, long RNA sequencing and microarray performed in this study have
598 been deposited to NCBI's Gene Expression Omnibus (GEO) database under the accession number
599 GSE174661 (Reviewer access with a token 'cvmpqccylxgnzgj') and GSE196773, respectively. In
600 addition, the analyzed dataset is presented with an online R Shiny app and can be accessed through a
601 browsable web portal (https://www.xulandenlab.com/humanwounds-mirna-mrna). The analysis source
602 code is available at https://github.com/Zhuang-Bio/miRNAprofiling.

603

604 **Competing Interest Statement**

605 The authors declare no conflict of interest.

606

607 **Funding and Acknowledgements**

608 We express our gratitude to the patients and healthy donors participating in this study. We thank Mona
609 Ståhle, Desiree Wiegleb Edström, Peter Berg, Fredrik Correa, Martin Gumulka, Mahsa Tayefi for clinical
610 sample collection; Helena Griehsel for technical support. We thank the Microarray core facility at Novum,
611 BEA, which is supported by the board of research at KI and the research committee at the Karolinska
612 hospital. The computations/data handling was enabled by resources in the projects sens2020010 and
613 2021/22-701 provided by the Swedish National Infrastructure for Computing (SNIC) at UPPMAX,
614 partially funded by the Swedish Research Council through grant agreement no. 2018-05973. This work
615 was supported by Swedish Research Council (Vetenskapsradet, 2016-02051 and 2020-01400), Ragnar
616 Söderbergs Foundation (M31/15), Welander and Finsens Foundation (Hudfonden), LEO foundation,
617 Ming Wai Lau Centre for Reparative Medicine, Karolinska Institutet, and R01AR073614 from
618 NIH/NIAMS (to MTC).

619

620 **Author Contributions**

621 N.X.L. and P.S. conceived and designed the study. P.S. collected most clinical samples with the
622 assistance of M.A.T.. L.Z., D.L., M.A.T., and X.B. performed the experiments. Z.L. and L.Z. carried out
623 bioinformatics analysis. I.P. and M.T.C contributed to data analyses and interpretation. Z.L., L.Z., and
624 N.X.L. wrote the manuscript, which was commented on by all authors.

625 **References**

626 Agarwal, V., Bell, G. W., Nam, J. W., & Bartel, D. P. (2015, Aug 12). Predicting effective microRNA target
627 sites in mammalian mRNAs. *Elife, 4*. https://doi.org/10.7554/eLife.05005

628
629 Blumberg, S. N., Maggi, J., Melamed, J., Golinko, M., Ross, F., & Chen, W. (2012, Dec). A histopathologic
630 basis for surgical debridement to promote healing of venous ulcers. *J Am Coll Surg, 215*(6), 751-757.
631 https://doi.org/10.1016/j.jamcollsurg.2012.08.008

632
633 Bolger, A. M., Lohse, M., & Usadel, B. (2014, Aug 1). Trimmomatic: a flexible trimmer for Illumina sequence
634 data. *Bioinformatics, 30*(15), 2114-2120. https://doi.org/10.1093/bioinformatics/btu170

635
636 Botchkarev, V. A. (2003, 2003/01/01/). Bone Morphogenetic Proteins and Their Antagonists in Skin and Hair
637 Follicle Biology. *Journal of Investigative Dermatology, 120*(1), 36-47.
638 https://doi.org/https://doi.org/10.1046/j.1523-1747.2003.12002.x

639
640 Cherone, J. M., Jorgji, V., & Burge, C. B. (2019). Cotargeting among microRNAs in the brain. *Genome*
641 *research, 29*(11), 1791-1804. https://doi.org/10.1101/gr.249201.119

642
643 Darwin, E., & Tomic-Canic, M. (2018, Dec). Healing Chronic Wounds: Current Challenges and Potential
644 Solutions. *Curr Dermatol Rep, 7*(4), 296-302. https://doi.org/10.1007/s13671-018-0239-4

645
646 Dobin, A., Davis, C. A., Schlesinger, F., Drenkow, J., Zaleski, C., Jha, S., Batut, P., Chaisson, M., & Gingeras,
647 T. R. (2013, Jan 1). STAR: ultrafast universal RNA-seq aligner. *Bioinformatics, 29*(1), 15-21.
648 https://doi.org/10.1093/bioinformatics/bts635

649
650 Elliot, S., Wikramanayake, T. C., Jozic, I., & Tomic-Canic, M. (2018, Apr). A Modeling Conundrum: Murine
651 Models for Cutaneous Wound Healing. *J Invest Dermatol, 138*(4), 736-740.
652 https://doi.org/10.1016/j.jid.2017.12.001

653
654 Eming, S. A., Martin, P., & Tomic-Canic, M. (2014, Dec 3). Wound repair and regeneration: mechanisms,
655 signaling, and translation. *Sci Transl Med, 6*(265), 265sr266.
656 https://doi.org/10.1126/scitranslmed.3009337

657
658 Erhard, F., Haas, J., Lieber, D., Malterer, G., Jaskiewicz, L., Zavolan, M., Dölken, L., & Zimmer, R. (2014).
659 Widespread context dependency of microRNA-mediated regulation. *Genome research, 24*(6), 906-919.
660 https://doi.org/10.1101/gr.166702.113

661
662 Ertosun, M. G., Hapil, F. Z., & Osman Nidai, O. (2016, 2016/10/01/). E2F1 transcription factor and its impact
663 on growth factor and cytokine signaling. *Cytokine & Growth Factor Reviews, 31*, 17-25.
664 https://doi.org/https://doi.org/10.1016/j.cytogfr.2016.02.001

665
666 Friedlander, M. R., Mackowiak, S. D., Li, N., Chen, W., & Rajewsky, N. (2012, Jan). miRDeep2 accurately
667 identifies known and hundreds of novel microRNA genes in seven animal clades. *Nucleic Acids Res,*
668 *40*(1), 37-52. https://doi.org/10.1093/nar/gkr688

669
670 Gu, Z., Eils, R., & Schlesner, M. (2016, Sep 15). Complex heatmaps reveal patterns and correlations in
671 multidimensional genomic data. *Bioinformatics, 32*(18), 2847-2849.
672 https://doi.org/10.1093/bioinformatics/btw313

Gu, Z., Gu, L., Eils, R., Schlesner, M., & Brors, B. (2014, Oct). circlize Implements and enhances circular visualization in R. *Bioinformatics, 30*(19), 2811-2812. https://doi.org/10.1093/bioinformatics/btu393

Guo, F., Carter, D. E., & Leask, A. (2014, Apr). miR-218 regulates focal adhesion kinase-dependent TGFβ signaling in fibroblasts. *Mol Biol Cell, 25*(7), 1151-1158. https://doi.org/10.1091/mbc.E13-08-0451

Guo, J., Zhang, J. F., Wang, W. M., Cheung, F. W., Lu, Y. F., Ng, C. F., Kung, H. F., & Liu, W. K. (2014). MicroRNA-218 inhibits melanogenesis by directly suppressing microphthalmia-associated transcription factor expression. *RNA Biol, 11*(6), 732-741. https://doi.org/10.4161/rna.28865

Hadley, W. (2016). ggplot2: Elegant Graphics for Data Analysis. *Springer-Verlag New York*. https://ggplot2.tidyverse.org

Han, H., Cho, J. W., Lee, S., Yun, A., Kim, H., Bae, D., Yang, S., Kim, C. Y., Lee, M., Kim, E., Lee, S., Kang, B., Jeong, D., Kim, Y., Jeon, H. N., Jung, H., Nam, S., Chung, M., Kim, J. H., & Lee, I. (2018, Jan 4). TRRUST v2: an expanded reference database of human and mouse transcriptional regulatory interactions. *Nucleic Acids Res, 46*(D1), D380-d386. https://doi.org/10.1093/nar/gkx1013

Herter, E. K., & Xu Landen, N. (2017, Mar 1). Non-Coding RNAs: New Players in Skin Wound Healing. *Adv Wound Care (New Rochelle), 6*(3), 93-107. https://doi.org/10.1089/wound.2016.0711

Hoversten, K. P., Kiemele, L. J., Stolp, A. M., Takahashi, P. Y., & Verdoorn, B. P. (2020, Sep). Prevention, Diagnosis, and Management of Chronic Wounds in Older Adults. *Mayo Clin Proc, 95*(9), 2021-2034. https://doi.org/10.1016/j.mayocp.2019.10.014

Ichihara, A., Jinnin, M., Yamane, K., Fujisawa, A., Sakai, K., Masuguchi, S., Fukushima, S., Maruo, K., & Ihn, H. (2011, Nov). microRNA-mediated keratinocyte hyperproliferation in psoriasis vulgaris. *Br J Dermatol, 165*(5), 1003-1010. https://doi.org/10.1111/j.1365-2133.2011.10497.x

Kaufman, C. K., Zhou, P., Pasolli, H. A., Rendl, M., Bolotin, D., Lim, K. C., Dai, X., Alegre, M. L., & Fuchs, E. (2003, Sep 1). GATA-3: an unexpected regulator of cell lineage determination in skin. *Genes Dev, 17*(17), 2108-2122. https://doi.org/10.1101/gad.1115203

Korotkevich, G., Sukhov, V., Budin, N., Shpak, B., Artyomov, M. N., & Sergushichev, A. (2021). Fast gene set enrichment analysis. *bioRxiv*, 060012. https://doi.org/10.1101/060012

Kozomara, A., Birgaoanu, M., & Griffiths-Jones, S. (2018). miRBase: from microRNA sequences to function. *Nucleic Acids Research, 47*(D1), D155-D162. https://doi.org/10.1093/nar/gky1141

Kurek, D., Garinis, G. A., van Doorninck, J. H., van der Wees, J., & Grosveld, F. G. (2007, Jan). Transcriptome and phenotypic analysis reveals Gata3-dependent signalling pathways in murine hair follicles. *Development, 134*(2), 261-272. https://doi.org/10.1242/dev.02721

Lai, X., Eberhardt, M., Schmitz, U., & Vera, J. (2019). Systems biology-based investigation of cooperating microRNAs as monotherapy or adjuvant therapy in cancer. *Nucleic Acids Research, 47*(15), 7753-7766. https://doi.org/10.1093/nar/gkz638

Landen, N. X., Li, D., & Stahle, M. (2016, Oct). Transition from inflammation to proliferation: a critical step during wound healing. *Cell Mol Life Sci, 73*(20), 3861-3885. https://doi.org/10.1007/s00018-016-2268-0

Langfelder, P., & Horvath, S. (2008, Dec 29). WGCNA: an R package for weighted correlation network analysis. *BMC Bioinformatics, 9*, 559. https://doi.org/10.1186/1471-2105-9-559

Langfelder, P., Luo, R., Oldham, M. C., & Horvath, S. (2011, Jan 20). Is my network module preserved and reproducible? *PLoS Comput Biol, 7*(1), e1001057. https://doi.org/10.1371/journal.pcbi.1001057

Langmead, B., Trapnell, C., Pop, M., & Salzberg, S. L. (2009, 2009/03/04). Ultrafast and memory-efficient alignment of short DNA sequences to the human genome. *Genome Biology, 10*(3), R25. https://doi.org/10.1186/gb-2009-10-3-r25

Lewis, B. P., Burge, C. B., & Bartel, D. P. (2005, 2005/01/14/). Conserved Seed Pairing, Often Flanked by Adenosines, Indicates that Thousands of Human Genes are MicroRNA Targets. *Cell, 120*(1), 15-20. https://doi.org/https://doi.org/10.1016/j.cell.2004.12.035

Lewis, C. J., Mardaryev, A. N., Poterlowicz, K., Sharova, T. Y., Aziz, A., Sharpe, D. T., Botchkareva, N. V., & Sharov, A. A. (2014, Mar). Bone morphogenetic protein signaling suppresses wound-induced skin repair by inhibiting keratinocyte proliferation and migration. *J Invest Dermatol, 134*(3), 827-837. https://doi.org/10.1038/jid.2013.419

Li, D., Wang, A., Liu, X., Meisgen, F., Grunler, J., Botusan, I. R., Narayanan, S., Erikci, E., Li, X., Blomqvist, L., Du, L., Pivarcsi, A., Sonkoly, E., Chowdhury, K., Catrina, S. B., Stahle, M., & Landen, N. X. (2015, Aug 3). MicroRNA-132 enhances transition from inflammation to proliferation during wound healing. *J Clin Invest, 125*(8), 3008-3026. https://doi.org/10.1172/JCI79052

Liang, L., Stone, R. C., Stojadinovic, O., Ramirez, H., Pastar, I., Maione, A. G., Smith, A., Yanez, V., Veves, A., Kirsner, R. S., Garlick, J. A., & Tomic-Canic, M. (2016, Nov). Integrative analysis of miRNA and mRNA paired expression profiling of primary fibroblast derived from diabetic foot ulcers reveals multiple impaired cellular functions. *Wound Repair Regen, 24*(6), 943-953. https://doi.org/10.1111/wrr.12470

Liang, P., Lv, C., Jiang, B., Long, X., Zhang, P., Zhang, M., Xie, T., & Huang, X. (2012, 2012/06/01/). MicroRNA profiling in denatured dermis of deep burn patients. *Burns, 38*(4), 534-540. https://doi.org/https://doi.org/10.1016/j.burns.2011.10.014

Liao, Y., Smyth, G. K., & Shi, W. (2013). featureCounts: an efficient general purpose program for assigning sequence reads to genomic features. *Bioinformatics, 30*(7), 923-930. https://doi.org/10.1093/bioinformatics/btt656

Liao, Y., Wang, J., Jaehnig, E. J., Shi, Z., & Zhang, B. (2019). WebGestalt 2019: gene set analysis toolkit with revamped UIs and APIs. *Nucleic Acids Research, 47*(W1), W199-W205. https://doi.org/10.1093/nar/gkz401

Liu, T., Zhang, L., Joo, D., & Sun, S.-C. (2017, 2017/07/14). NF-κB signaling in inflammation. *Signal Transduction and Targeted Therapy, 2*(1), 17023. https://doi.org/10.1038/sigtrans.2017.23

Love, M. I., Huber, W., & Anders, S. (2014, 2014/12/05). Moderated estimation of fold change and dispersion for RNA-seq data with DESeq2. *Genome Biology, 15*(12), 550. https://doi.org/10.1186/s13059-014-0550-8

Luan, A., Hu, M. S., Leavitt, T., Brett, E. A., Wang, K. C., Longaker, M. T., & Wan, D. C. (2018, Jan 1). Noncoding RNAs in Wound Healing: A New and Vast Frontier. *Adv Wound Care (New Rochelle), 7*(1), 19-27. https://doi.org/10.1089/wound.2017.0765

Mackowiak, S. D. (2011, Dec). Identification of novel and known miRNAs in deep-sequencing data with miRDeep2. *Curr Protoc Bioinformatics, Chapter 12*, Unit 12 10. https://doi.org/10.1002/0471250953.bi1210s36

Meng, Z., Zhou, D., Gao, Y., Zeng, M., & Wang, W. (2018, Apr). miRNA delivery for skin wound healing. *Adv Drug Deliv Rev, 129*, 308-318. https://doi.org/10.1016/j.addr.2017.12.011

Nakashima, T., Jinnin, M., Etoh, T., Fukushima, S., Masuguchi, S., Maruo, K., Inoue, Y., Ishihara, T., & Ihn, H. (2010, Dec 14). Down-regulation of mir-424 contributes to the abnormal angiogenesis via MEK1 and cyclin E1 in senile hemangioma: its implications to therapy. *PLoS One, 5*(12), e14334. https://doi.org/10.1371/journal.pone.0014334

Nie, X., Zhao, J., Ling, H., Deng, Y., Li, X., & He, Y. (2020, Sep). Exploring microRNAs in diabetic chronic cutaneous ulcers: Regulatory mechanisms and therapeutic potential. *Br J Pharmacol, 177*(18), 4077-4095. https://doi.org/10.1111/bph.15139

Nielsen, M. M., & Pedersen, J. S. (2020). miRNA activity inferred from single cell mRNA expression. *bioRxiv*, 2020.2007.2014.202051. https://doi.org/10.1101/2020.07.14.202051

Pachera, E., Assassi, S., Salazar, G. A., Stellato, M., Renoux, F., Wunderlin, A., Blyszczuk, P., Lafyatis, R., Kurreeman, F., de Vries-Bouwstra, J., Messemaker, T., Feghali-Bostwick, C. A., Rogler, G., van Haaften, W. T., Dijkstra, G., Oakley, F., Calcagni, M., Schniering, J., Maurer, B., Distler, J. H., Kania, G., Frank-Bertoncelj, M., & Distler, O. (2020, Sep 1). Long noncoding RNA H19X is a key mediator of TGF-beta-driven fibrosis. *J Clin Invest, 130*(9), 4888-4905. https://doi.org/10.1172/JCI135439

Pappas, P. J., You, R., Rameshwar, P., Gorti, R., DeFouw, D. O., Phillips, C. K., Padberg, F. T., Jr., Silva, M. B., Jr., Simonian, G. T., Hobson, R. W., 2nd, & Duran, W. N. (1999, Dec). Dermal tissue fibrosis in patients with chronic venous insufficiency is associated with increased transforming growth factor-beta1 gene expression and protein production. *J Vasc Surg, 30*(6), 1129-1145. https://doi.org/10.1016/s0741-5214(99)70054-6

Pastar, I., Marjanovic, J., Stone, R. C., Chen, V., Burgess, J. L., Mervis, J. S., & Tomic-Canic, M. (2021, Mar 10). Epigenetic regulation of cellular functions in wound healing. *Exp Dermatol*. https://doi.org/10.1111/exd.14325

Pastar, I., Wong, L. L., Egger, A. N., & Tomic-Canic, M. (2018, May). Descriptive vs mechanistic scientific approach to study wound healing and its inhibition: Is there a value of translational research involving human subjects? *Exp Dermatol, 27*(5), 551-562. https://doi.org/10.1111/exd.13663

Ramirez, H. A., Pastar, I., Jozic, I., Stojadinovic, O., Stone, R. C., Ojeh, N., Gil, J., Davis, S. C., Kirsner, R. S., & Tomic-Canic, M. (2018, May). Staphylococcus aureus Triggers Induction of miR-15B-5P to

821 Diminish DNA Repair and Deregulate Inflammatory Response in Diabetic Foot Ulcers. *J Invest*
822 *Dermatol, 138*(5), 1187-1196. https://doi.org/10.1016/j.jid.2017.11.038

823
824 Reinke, J. M., & Sorg, H. (2012). Wound repair and regeneration. *Eur Surg Res, 49*(1), 35-43.
825 https://doi.org/10.1159/000339613

826
827 Ritchie, M. E., Phipson, B., Wu, D., Hu, Y., Law, C. W., Shi, W., & Smyth, G. K. (2015). limma powers
828 differential expression analyses for RNA-sequencing and microarray studies. *Nucleic Acids Research,*
829 *43*(7), e47-e47. https://doi.org/10.1093/nar/gkv007

830
831 Ru, Y., Kechris, K. J., Tabakoff, B., Hoffman, P., Radcliffe, R. A., Bowler, R., Mahaffey, S., Rossi, S., Calin,
832 G. A., Bemis, L., & Theodorescu, D. (2014). The multiMiR R package and database: integration of
833 microRNA–target interactions along with their disease and drug associations. *Nucleic Acids Research,*
834 *42*(17), e133-e133. https://doi.org/10.1093/nar/gku631

835
836 Rupaimoole, R., & Slack, F. J. (2017, Mar). MicroRNA therapeutics: towards a new era for the management of
837 cancer and other diseases. *Nat Rev Drug Discov, 16*(3), 203-222. https://doi.org/10.1038/nrd.2016.246
838

839
840 Segre, J. A., Bauer, C., & Fuchs, E. (1999, 1999/08/01). Klf4 is a transcription factor required for establishing
841 the barrier function of the skin. *Nature Genetics, 22*(4), 356-360. https://doi.org/10.1038/11926

842
843 Sen, C. K., & Roy, S. (2012, Dec). OxymiRs in cutaneous development, wound repair and regeneration. *Semin*
844 *Cell Dev Biol, 23*(9), 971-980. https://doi.org/10.1016/j.semcdb.2012.09.012

845
846 Shannon, P., Markiel, A., Ozier, O., Baliga, N. S., Wang, J. T., Ramage, D., Amin, N., Schwikowski, B., &
847 Ideker, T. (2003, Nov). Cytoscape: a software environment for integrated models of biomolecular
848 interaction networks. *Genome Res, 13*(11), 2498-2504. https://doi.org/10.1101/gr.1239303

849
850 Shen, Z., Sun, J., Shao, J., & Xu, J. (2020). Ultraviolet B irradiation enhances the secretion of exosomes by
851 human primary melanocytes and changes their exosomal miRNA profile. *PLoS One, 15*(8), e0237023.
852 https://doi.org/10.1371/journal.pone.0237023

853
854 Stavast, C. J., & Erkeland, S. J. (2019). The Non-Canonical Aspects of MicroRNAs: Many Roads to Gene
855 Regulation. *Cells, 8*(11), 1465. https://doi.org/10.3390/cells8111465

856
857 Stojadinovic, O., Pastar, I., Nusbaum, A. G., Vukelic, S., Krzyzanowska, A., & Tomic-Canic, M. (2014, Mar-
858 Apr). Deregulation of epidermal stem cell niche contributes to pathogenesis of nonhealing venous
859 ulcers. *Wound Repair Regen, 22*(2), 220-227. https://doi.org/10.1111/wrr.12142

860
861 Stojadinovic, O., Pastar, I., Vukelic, S., Mahoney, M. G., Brennan, D., Krzyzanowska, A., Golinko, M., Brem,
862 H., & Tomic-Canic, M. (2008, Dec). Deregulation of keratinocyte differentiation and activation: a
863 hallmark of venous ulcers. *J Cell Mol Med, 12*(6b), 2675-2690. https://doi.org/10.1111/j.1582-
864 4934.2008.00321.x

865
866 Stone, R. C., Stojadinovic, O., Rosa, A. M., Ramirez, H. A., Badiavas, E., Blumenberg, M., & Tomic-Canic, M.
867 (2017, Jan 4). A bioengineered living cell construct activates an acute wound healing response in
868 venous leg ulcers. *Sci Transl Med, 9*(371). https://doi.org/10.1126/scitranslmed.aaf8611

869

Stone, R. C., Stojadinovic, O., Sawaya, A. P., Glinos, G. D., Lindley, L. E., Pastar, I., Badiavas, E., & Tomic-Canic, M. (2020, Mar). A bioengineered living cell construct activates metallothionein/zinc/MMP8 and inhibits TGFβ to stimulate remodeling of fibrotic venous leg ulcers. *Wound Repair Regen, 28*(2), 164-176. https://doi.org/10.1111/wrr.12778

Subramanian, A., Tamayo, P., Mootha, V. K., Mukherjee, S., Ebert, B. L., Gillette, M. A., Paulovich, A., Pomeroy, S. L., Golub, T. R., Lander, E. S., & Mesirov, J. P. (2005, Oct 25). Gene set enrichment analysis: a knowledge-based approach for interpreting genome-wide expression profiles. *Proc Natl Acad Sci U S A, 102*(43), 15545-15550. https://doi.org/10.1073/pnas.0506580102

[Record #219 is using a reference type undefined in this output style.]

Tong, Z., Cui, Q., Wang, J., & Zhou, Y. (2019, Jan 8). TransmiR v2.0: an updated transcription factor-microRNA regulation database. *Nucleic Acids Res, 47*(D1), D253-d258. https://doi.org/10.1093/nar/gky1023

Vivas, A., Lev-Tov, H., & Kirsner, R. S. (2016, Aug 2). Venous Leg Ulcers. *Ann Intern Med, 165*(3), Itc17-itc32. https://doi.org/10.7326/aitc201608020

Wu, J., Li, X., Li, D., Ren, X., Li, Y., Herter, E. K., Qian, M., Toma, M. A., Wintler, A. M., Serezal, I. G., Rollman, O., Stahle, M., Wikstrom, J. D., Ye, X., & Landen, N. X. (2020, Feb). MicroRNA-34 Family Enhances Wound Inflammation by Targeting LGR4. *J Invest Dermatol, 140*(2), 465-476 e411. https://doi.org/10.1016/j.jid.2019.07.694

Wu, Y. E., Parikshak, N. N., Belgard, T. G., & Geschwind, D. H. (2016, Nov). Genome-wide, integrative analysis implicates microRNA dysregulation in autism spectrum disorder. *Nat Neurosci, 19*(11), 1463-1476. https://doi.org/10.1038/nn.4373

Yang, L., Dai, J., Li, F., Cheng, H., Yan, D., & Ruan, Q. (2017, Sep 19). The expression and function of miR-424 in infantile skin hemangioma and its mechanism. *Sci Rep, 7*(1), 11846. https://doi.org/10.1038/s41598-017-10674-7

Zhang, B., & Horvath, S. (2005). A general framework for weighted gene co-expression network analysis. *Stat Appl Genet Mol Biol, 4*, Article17. https://doi.org/10.2202/1544-6115.1128

Zhao, B., Chen, Y., Yang, N., Chen, Q., Bao, Z., Liu, M., Hu, S., Li, J., & Wu, X. (2019, Nov). miR-218-5p regulates skin and hair follicle development through Wnt/β-catenin signaling pathway by targeting SFRP2. *J Cell Physiol, 234*(11), 20329-20341. https://doi.org/10.1002/jcp.28633

Zhou, L., Chen, J., Li, Z., Li, X., Hu, X., Huang, Y., Zhao, X., Liang, C., Wang, Y., Sun, L., Shi, M., Xu, X., Shen, F., Chen, M., Han, Z., Peng, Z., Zhai, Q., Chen, J., Zhang, Z., Yang, R., Ye, J., Guan, Z., Yang, H., Gui, Y., Wang, J., Cai, Z., & Zhang, X. (2010, Dec 30). Integrated profiling of microRNAs and mRNAs: microRNAs located on Xq27.3 associate with clear cell renal cell carcinoma. *PLoS One, 5*(12), e15224. https://doi.org/10.1371/journal.pone.0015224

916 **Figures with legends**

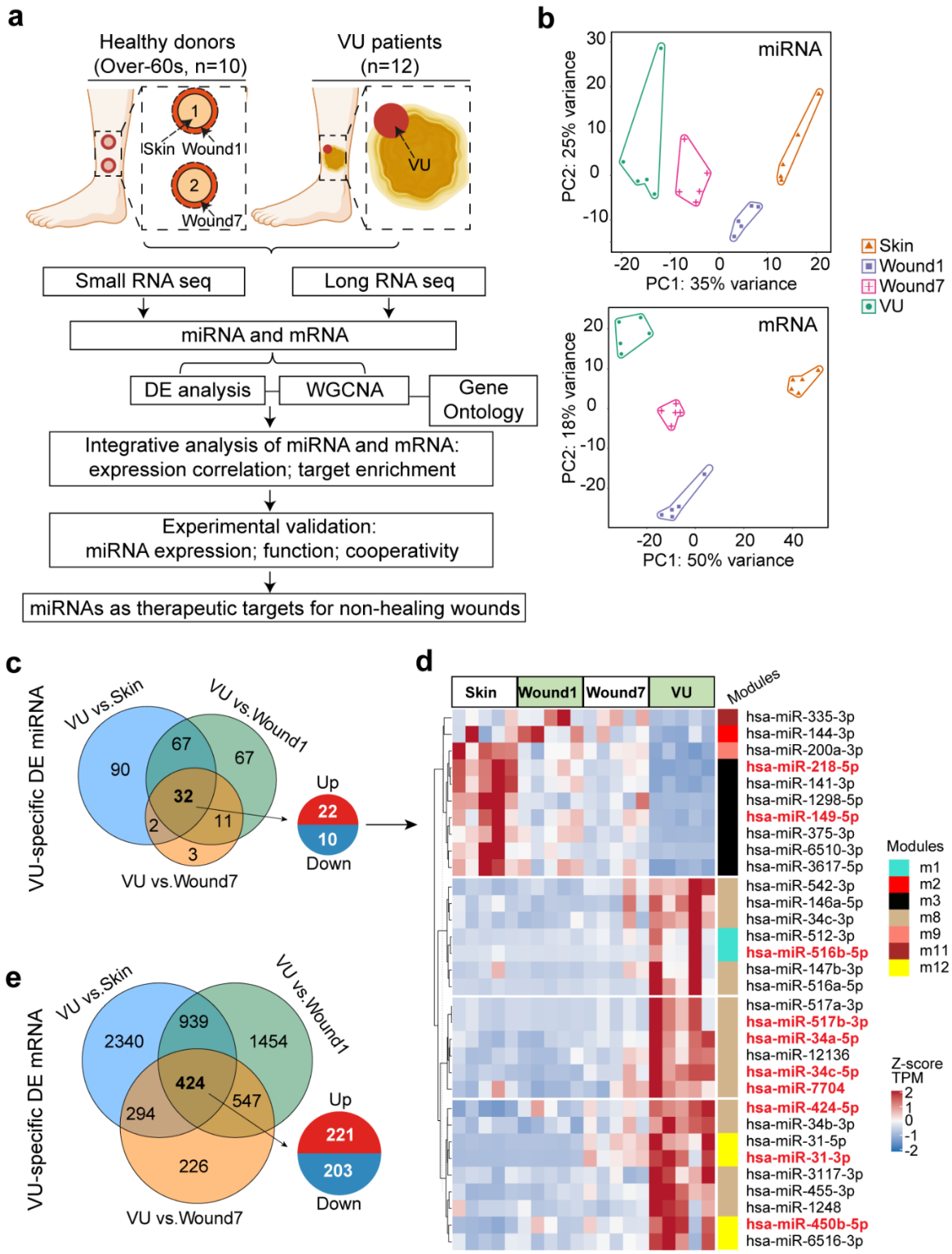

917

918 **Figure 1 Paired profiling of miRNA and mRNA expression in human wounds.** a Schematic of
919 analysis in this study. **b** PCA plots based on miRNA (upper panel) and mRNA (lower panel) expression
920 profiles. Each dot indicates an individual sample. The numbers of differentially expressed (DE) miRNAs

921 **c** and mRNAs **e** in VU (n=5) compared to the Skin, Wound1, and Wound7 from 5 healthy donors are
922 shown in Venn diagrams. FDR < 0.05, fold change ≥ 2 for miRNAs and ≥ 1.5 for mRNAs. **d** The heatmap
923 depicts the 32 miRNAs specifically dysregulated in the VU with scaled expression values (Z-scores).
924 WGCNA modules of each miRNA belongs to are marked with color bars. The miRNAs with
925 experimentally validated expression changes are highlighted in red.

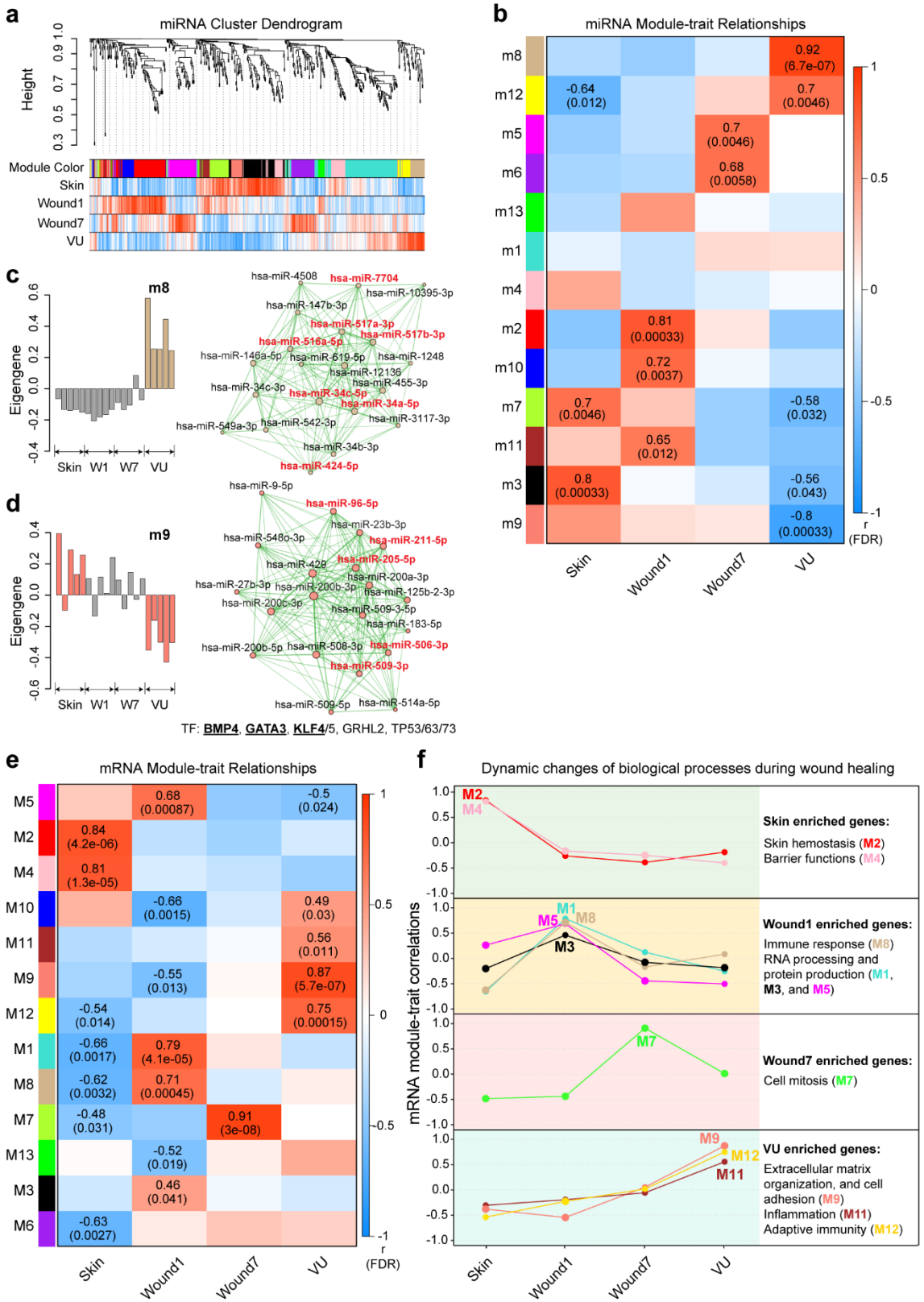

Figure 2 Weighted gene co-expression network analysis (WGCNA) of miRNAs and mRNAs in wound healing. a Cluster dendrogram shows miRNA co-expression modules: each branch corresponds to a module, and each leaf indicates a single miRNA. Color bars below show the module

930 assignment (the 1st row) and Pearson correlation coefficients between miRNA expression and the
931 sample groups (the 2nd to the 5th row: red and blue lines represent positive and negative correlations,
932 respectively). **b** Heatmap shows Pearson correlations between miRNA module eigengenes (ME) and
933 the sample groups. The correlation coefficients and the adjusted *P-values* (FDR) are shown where the
934 FDRs are less than 0.05. For the VU-associated modules m8 **c** and m9 **d**, bar plots (left) depict the ME
935 values across the 20 samples analyzed by RNA-seq, and network plots (right) show the top 20 miRNAs
936 with the highest kME values in each module. Node size and edge thickness are proportional to the kME
937 values and the weighted correlations between two connected miRNAs, respectively. The miRs with their
938 targetome enriched with VU-mRNA signature (see **Figure 4b**) are highlighted in red. Transcription
939 factors (TFs) with their targets enriched in the m9 module (Fisher's exact test: FDR < 0.05) are listed
940 below the network, and TFs differentially expressed in VU are underlined. **e** Heatmap shows Pearson
941 correlations between mRNA MEs and the sample groups. **f** The gene expression pattern of each
942 module across all the sample groups is depicted with line charts. Gene ontology analysis of biological
943 processes enriched in each module is shown at the right.

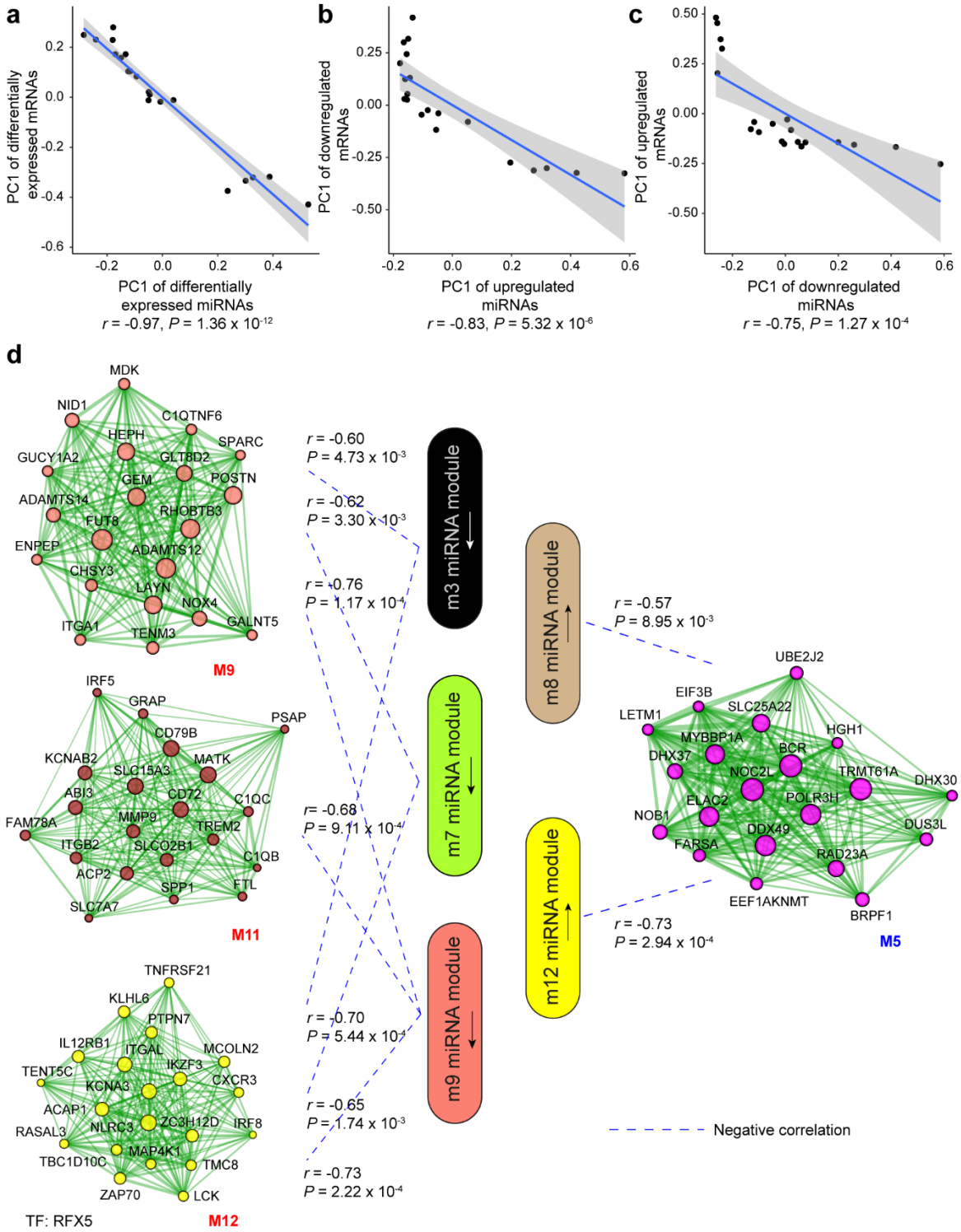

Figure 3 Correlation analysis between miRNA and mRNA expression changes in VU. a-c Correlations between the first principal component (PC1) of VU-associated differentially expressed (DE) miRNAs, and the PC1 of VU DE mRNAs predicted as miRNA targets. **d** PC1 correlations between the hub miRNAs and their predicted targets in the VU-associated miRNA and mRNA modules. Pearson

949 correlation coefficients (*r*) and *P* values are shown. The mRNA networks are plotted with the top 20
950 most connected module genes. Transcription factors (TFs) with targets enriched in the VU-associated
951 modules are listed below the networks.

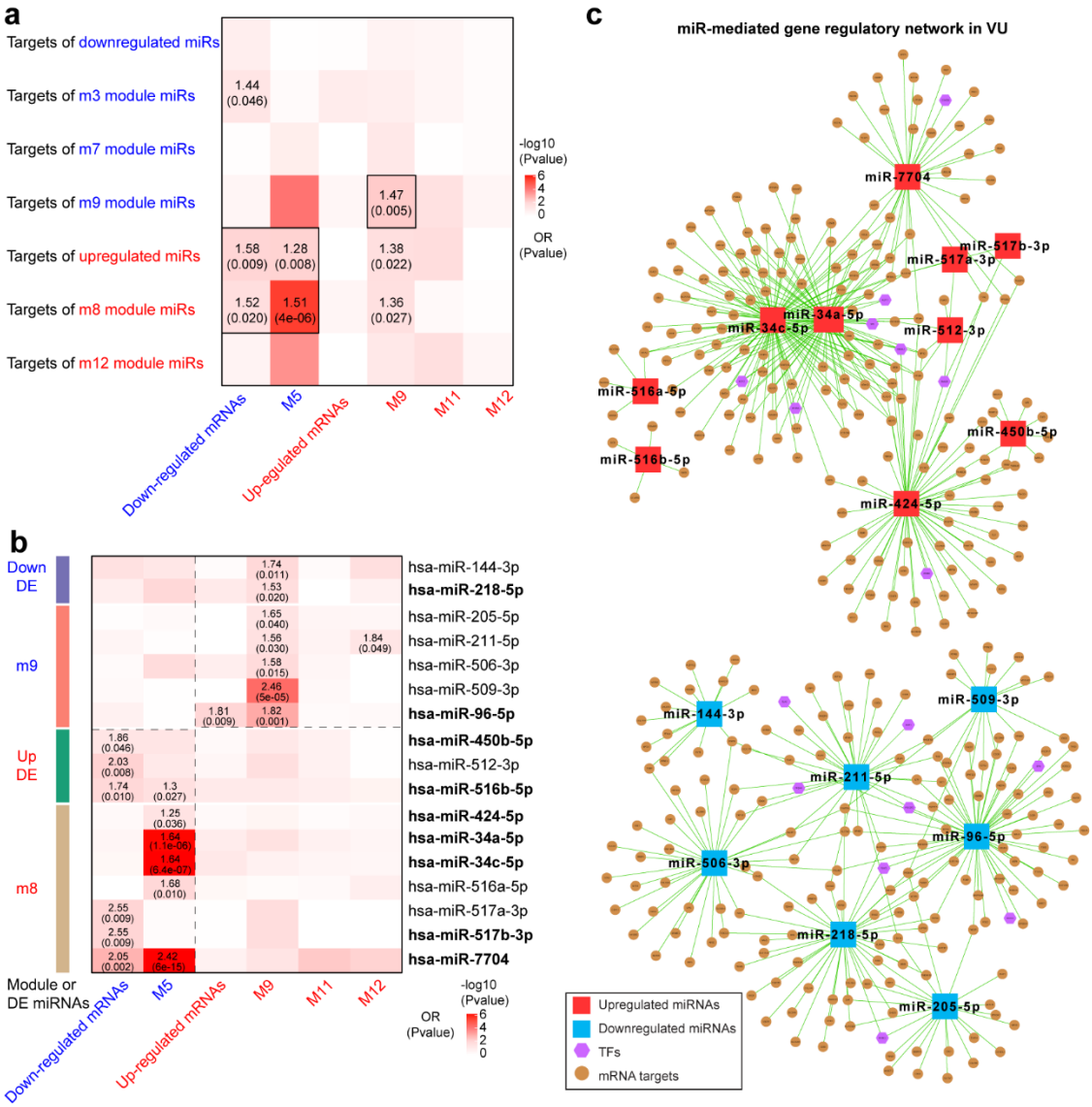

Figure 4 Integrative analysis of miRNA and mRNA expression changes in VU. Heatmaps show the enrichment for VU-affected mRNAs and mRNA modules in the top targets of **a** VU-associated DE miRNAs and miR modules and **b** the individual candidate miRNAs. Odds ratio (OR) and *P* values are indicated when OR > 1 and *P-value* < 0.05 (Fisher's exact test). The miRNAs with experimentally validated expression changes are highlighted in bold. **c** miR-mediated gene regulatory networks in VU are constructed with the miRNAs in **Figure 4b**, the mRNAs predicted as the strongest targets and with anti-correlated expression patterns (Pearson correlation, *P-value* < 0.05 and r < 0) with these miRNAs in human wounds, and the TFs regulating these miRNAs' expression from the TransmiR v2 database. An enlarged version of these networks can be found in **Figure 4 – figure supplement 1 and 2**.

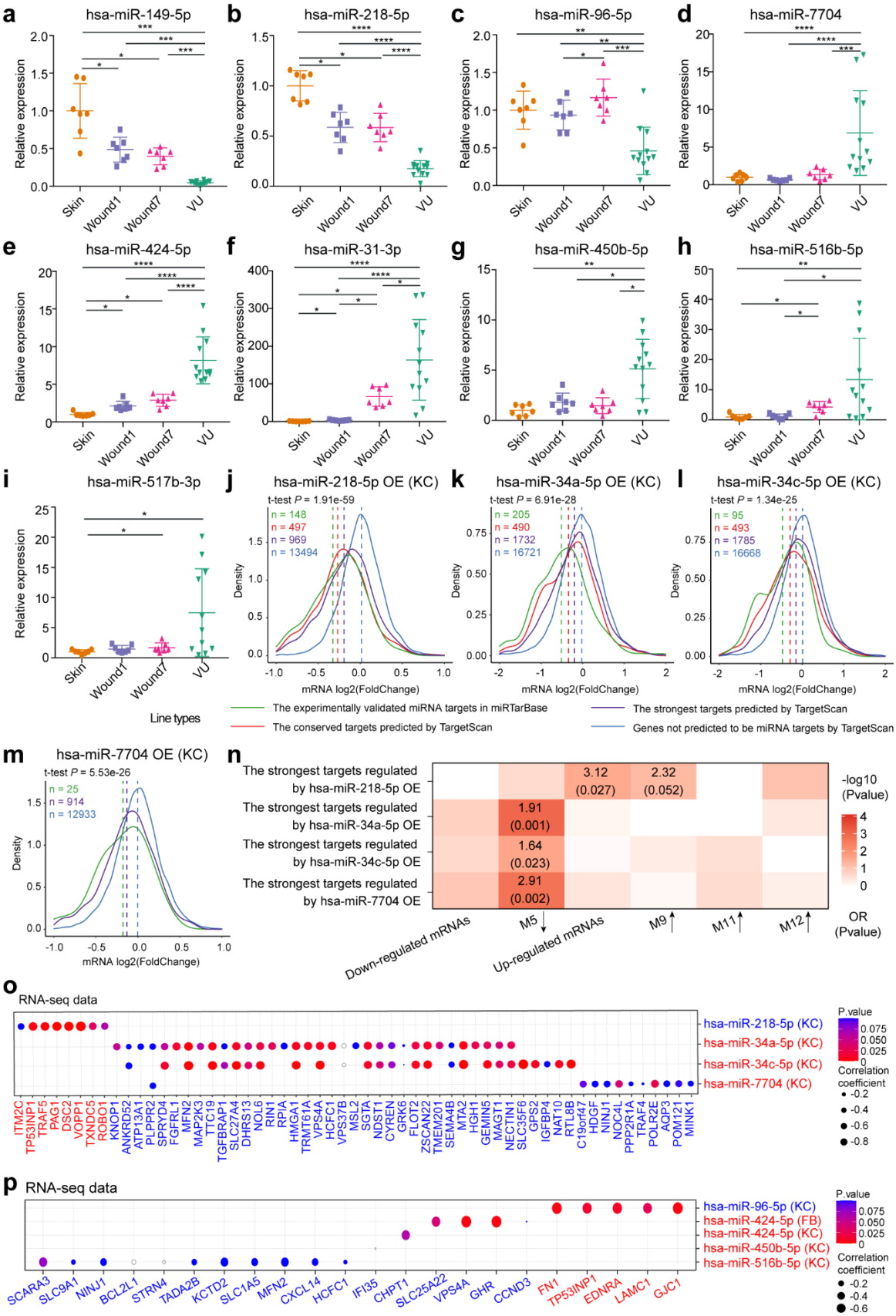

963

964 **Figure 5 Experimental validation of miRNAs' expression and targets in human skin wounds. a-i**

965 qRT-PCR analysis of VU-associated DE miRNAs in the skin, day 1 and day 7 acute wounds from 7
966 healthy donors and venous ulcers (VU) from 12 patients. Wilcoxon signed-rank test was used for the
967 comparison between Skin, Wound1, and Wound7; Mann-Whitney U test was used for comparing VU
968 with the skin and acute wounds. *$P < 0.05$, **$P < 0.01$, ***$P < 0.001$, ****$P < 0.0001$. **j-m** Microarray
969 analysis was performed in keratinocytes (KC) with miR-218-5p (**J**), miR-34a-5p **k**, miR-34c-5p **l**, or miR-
970 7704 **m** overexpression (OE), and density plots of mRNAs $\log_2$(fold change) are shown. Wilcoxon t-
971 tests were performed to compare the TargetScan predicted strongest targets (purple) with the non-
972 targets (blue) for each of these miRNAs. The conserved and experimentally validated targets are
973 marked with red and green colors, respectively. Dotted lines depict the average log2(fold change)
974 values for each mRNA group. **n** A heatmap shows the enrichment for VU-affected mRNAs and mRNA
975 modules in the targets of miR-218-5p, miR-34a-5p, miR-34c-5p, or miR-7704 validated by the
976 microarray analysis. Odds ratio (OR) and *P* values are shown when OR > 1 and *P-value* < 0.05 (Fisher's
977 exact test). **o, p** For each of the miRNAs (miR-218-5p, miR-34a-5p, miR-34c-5p, miR-7704, miR-96,
978 miR-424, miR-450b, and miR-516b) and its targets validated by the microarray analysis of KC or
979 fibroblasts (FB), Pearson correlation analysis was performed between their expression values in human
980 skin and wound samples shown by RNA-seq. Grey circles indicate correlation coefficients > 0.

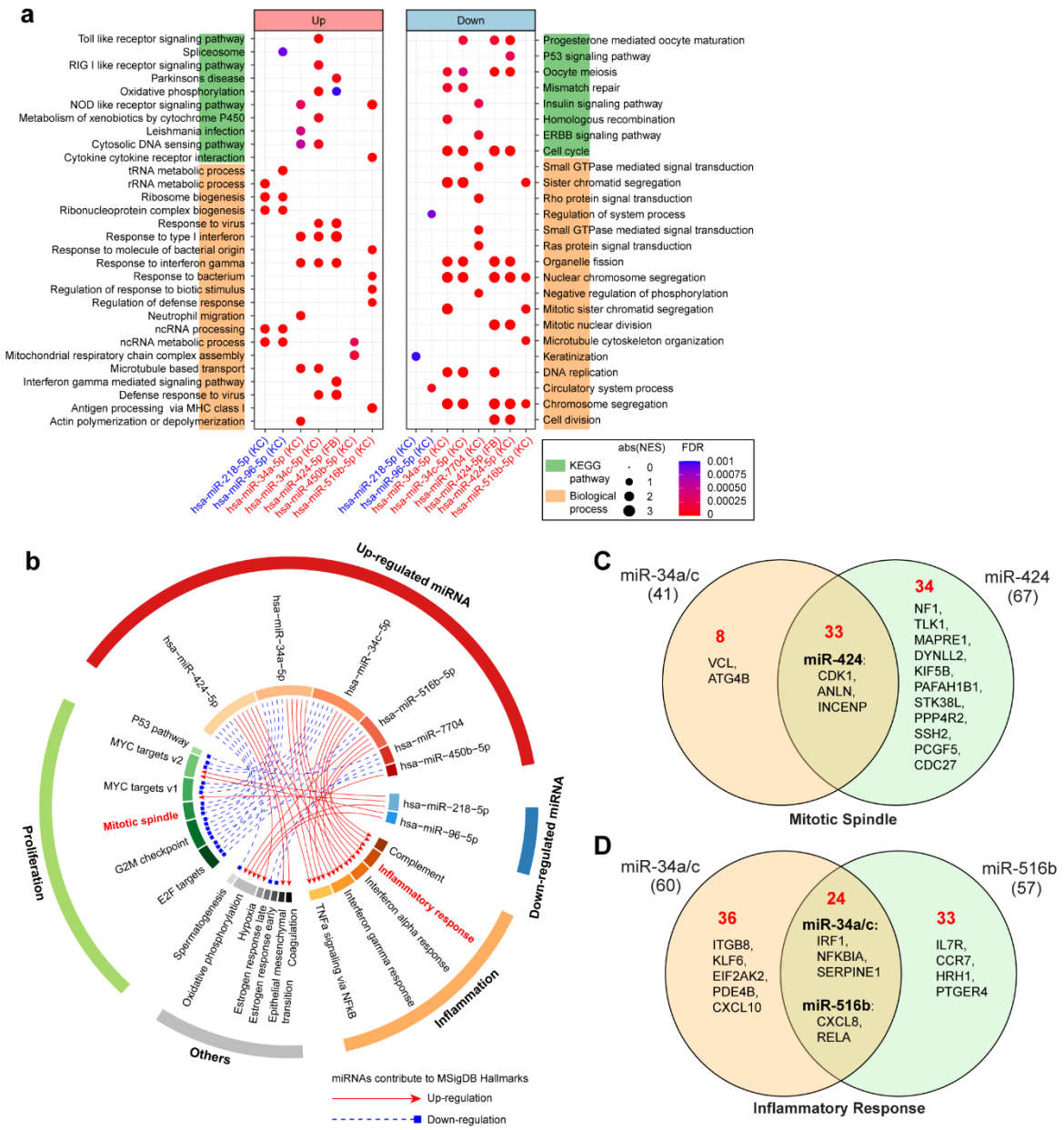

Figure 6 Cooperativity of VU pathology-relevant miRNAs. For the microarray data in keratinocytes (KC) or fibroblasts (FB) with miR-218-5p, miR-96-5p, miR-34a-5p, miR-34c-5p, miR-7704, miR-424-5p, miR-516-5p overexpression, we analyzed KEGG pathways, biological processes **a**, and Molecular Signatures Database (MSigDB) hallmarks **b** enriched by the genes up-or down-regulated by these miRNAs. Venn diagrams show the numbers of the mitotic spindle-related genes regulated by miR-34a/c-5p and miR-424-5p **c** and the inflammatory response-related genes regulated by miR-34a/c-5p and miR-516b-5p **d** (fold change > 1.2, *P*-value < 0.05) in the microarray analysis of keratinocytes

989 overexpressing these miRNAs. Among the regulated genes, the targets of each miRNA are depicted in
990 the plots.

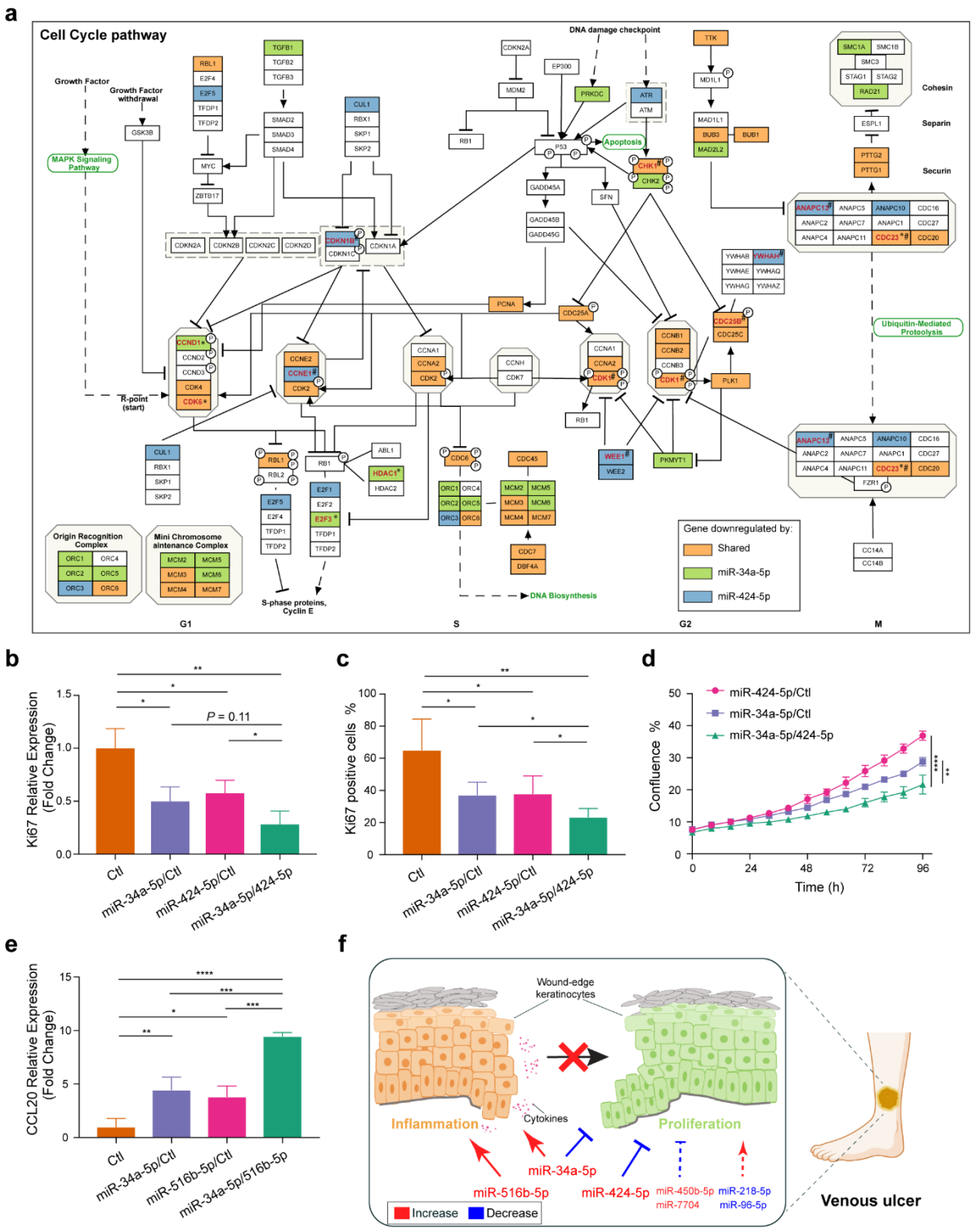

Figure 7 Cooperation of miR-34a, miR-424, and miR-516 in regulating keratinocyte proliferation and inflammatory response. a In the KEGG cell cycle pathway map, genes regulated by miR-34a-5p or miR-424-5p or both miRNAs as shown in the microarray analysis of keratinocytes are marked with green, blue, and orange colors, respectively. Among the regulated genes, the miRNA targets are

996 highlighted in red and labeled with * for miR-34a targets, # for miR-424 targets, *# for the gene co-
997 targeted by both miRNAs. Ki67 expression was detected in keratinocytes transfected with miR-34a-5p
998 or miR-424-5p mimics alone or both mimics for 24 hours (n = 3) by qRT-PCR **b** and
999 immunofluorescence staining (n = 5 for Ctl and miR-34a-5p/424-5p, n = 4 for miR-34a-5p/ctl and miR-
1000 424-5p/ctl) **c**. **d** The growth of the transfected keratinocytes (n = 3) was analyzed with a live cell imaging
1001 system. **e** qRT-PCR analysis of CCL20 in keratinocytes transfected with miR-34a-5p or miR-516b-5p
1002 mimics alone or both mimics for 24 hours (n = 3). **f** Proposed mechanism by which VU-dysregulated
1003 miRNAs cooperatively contribute to the stalled wound healing characterized with failed inflammation-
1004 proliferation transition. *P < 0.05; **P < 0.01; ***P < 0.001 and ****P<0.0001 by unpaired two-tailed
1005 Student's t-test **b, c,** and **e** and Two-way ANOVA **e**. Data are presented as mean ± SD.

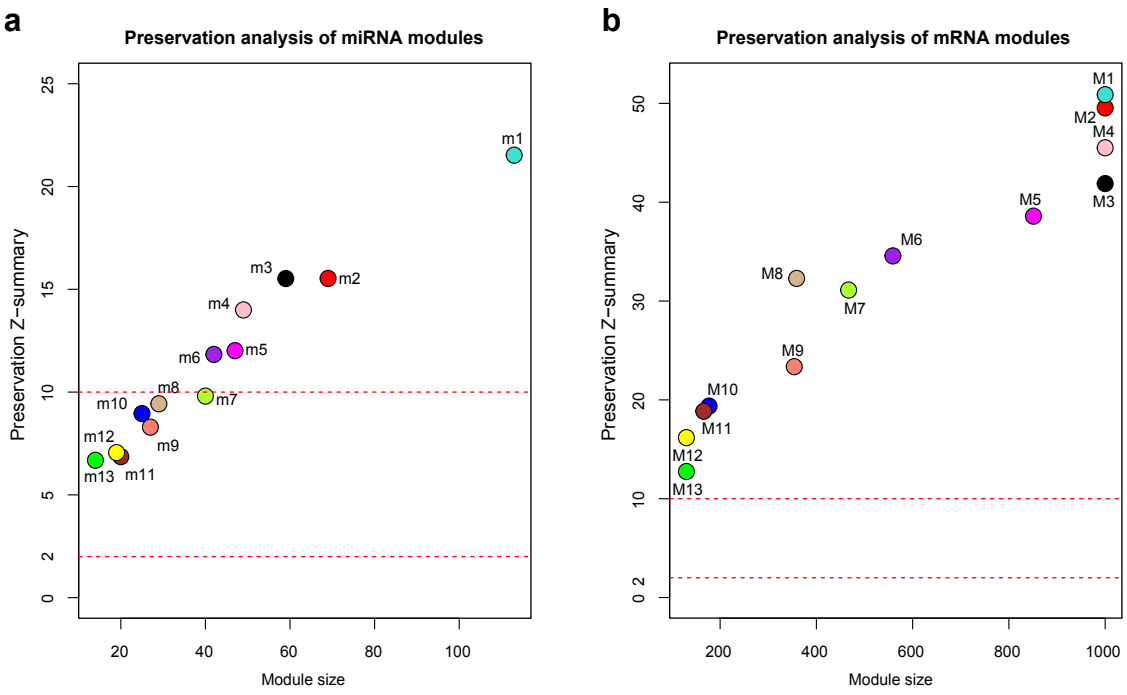

Figure 2 - figure supplement 1 Preservation analysis of miRNA a and mRNA b co-expression modules. The standardized Z-scores were calculated for each module by permutating 200 times using the 20 samples analyzed by RNA-seq as reference and test datasets. Modular preservation is strong if Z-summary > 10, weak to moderate if 2 < Z-summary < 10, no evidence of preservation if Z-summary ≤ 2. miRNA modules.

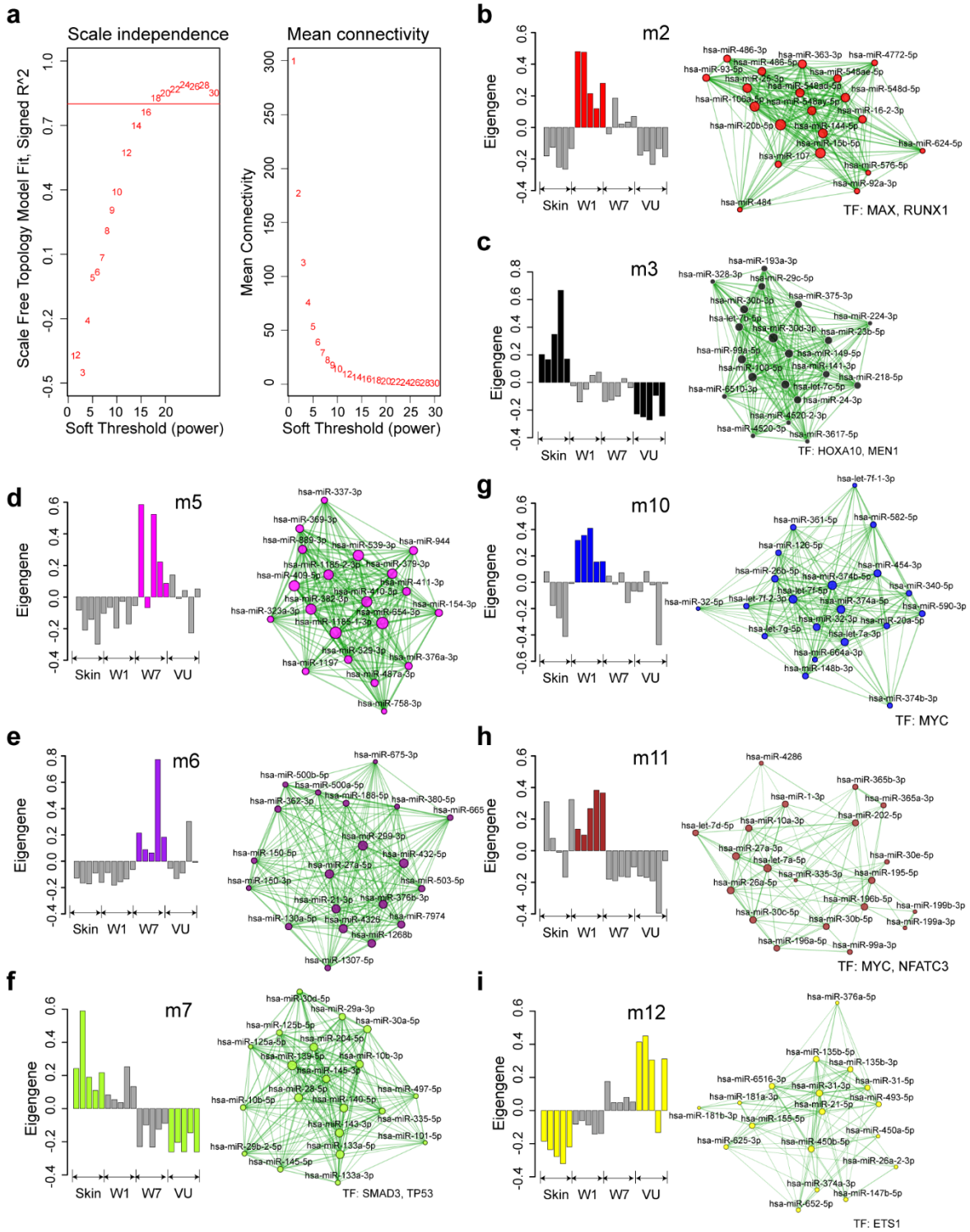

Figure 2 - figure supplement 2 Weighted gene co-expression network analysis (WGCNA) of miRNAs in human skin wound healing (related to **Figure 2a–d**). **a** The scale-free topology fit index (left) and mean connectivity (right) for various soft-threshold powers. The red line indicates signed R^2 = 0.8. **b–i** Bar plots (left) depict the ME values across the 20 samples analyzed by RNA-seq and network plots (right) show the top 20 miRNAs with the highest kME values in each module. Node size and edge

1018 thickness are proportional to the kME values and the weighted correlations between two connected
1019 miRNAs, respectively. Transcription factors (TFs) with their targets enriched in the modules (Fisher's
1020 exact test: FDR < 0.05) are listed below the networks.

1021

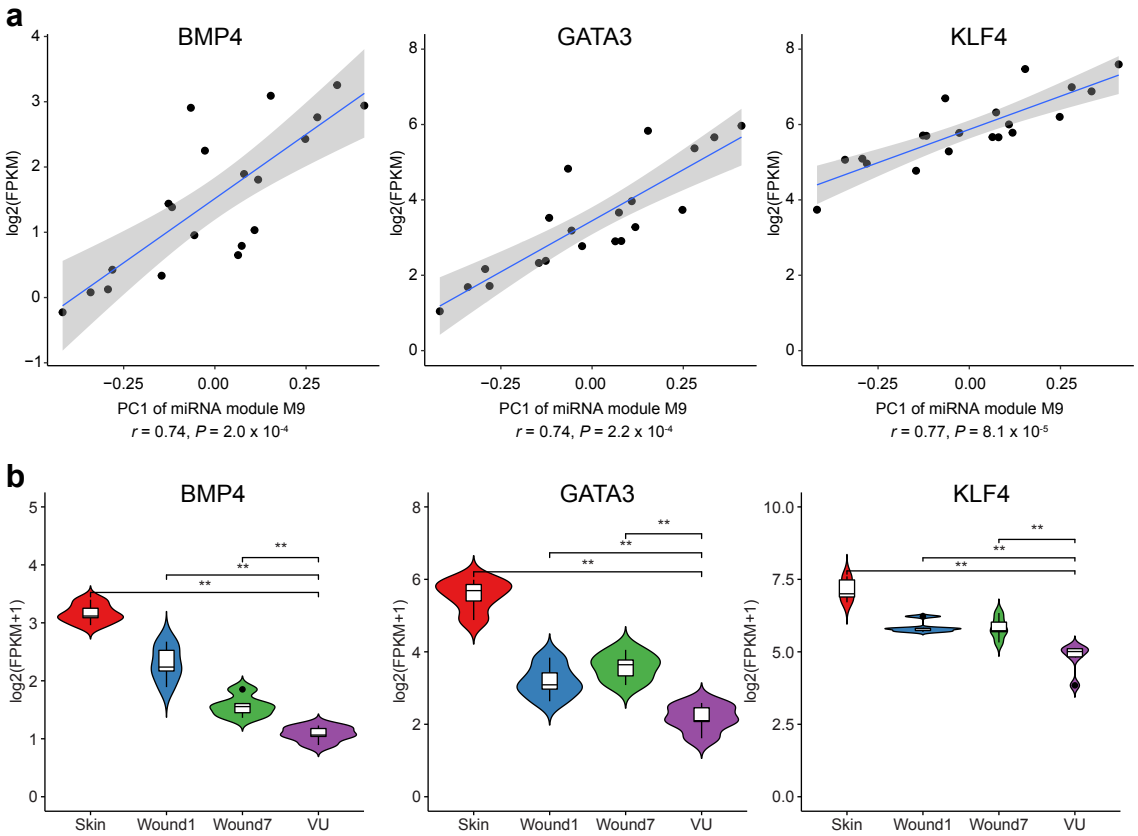

1022

1023 **Figure 2 - figure supplement 3 Transcription factors (TFs) with targets enriched in the miRNA**
1024 **m9 module. a** Pearson correlations between the first principal component (PC1) of miRNAs module
1025 m9 and the expression of BMP4, GATA3, or KLF4. **b** BMP4, GATA3, and KLF4 expression in the skin,
1026 day 1 and day 7 acute wounds from five healthy donors and in five venous ulcers analyzed by RNA-
1027 sequencing. Mann-Whitney t-test, $^{**}P < 0.01$.

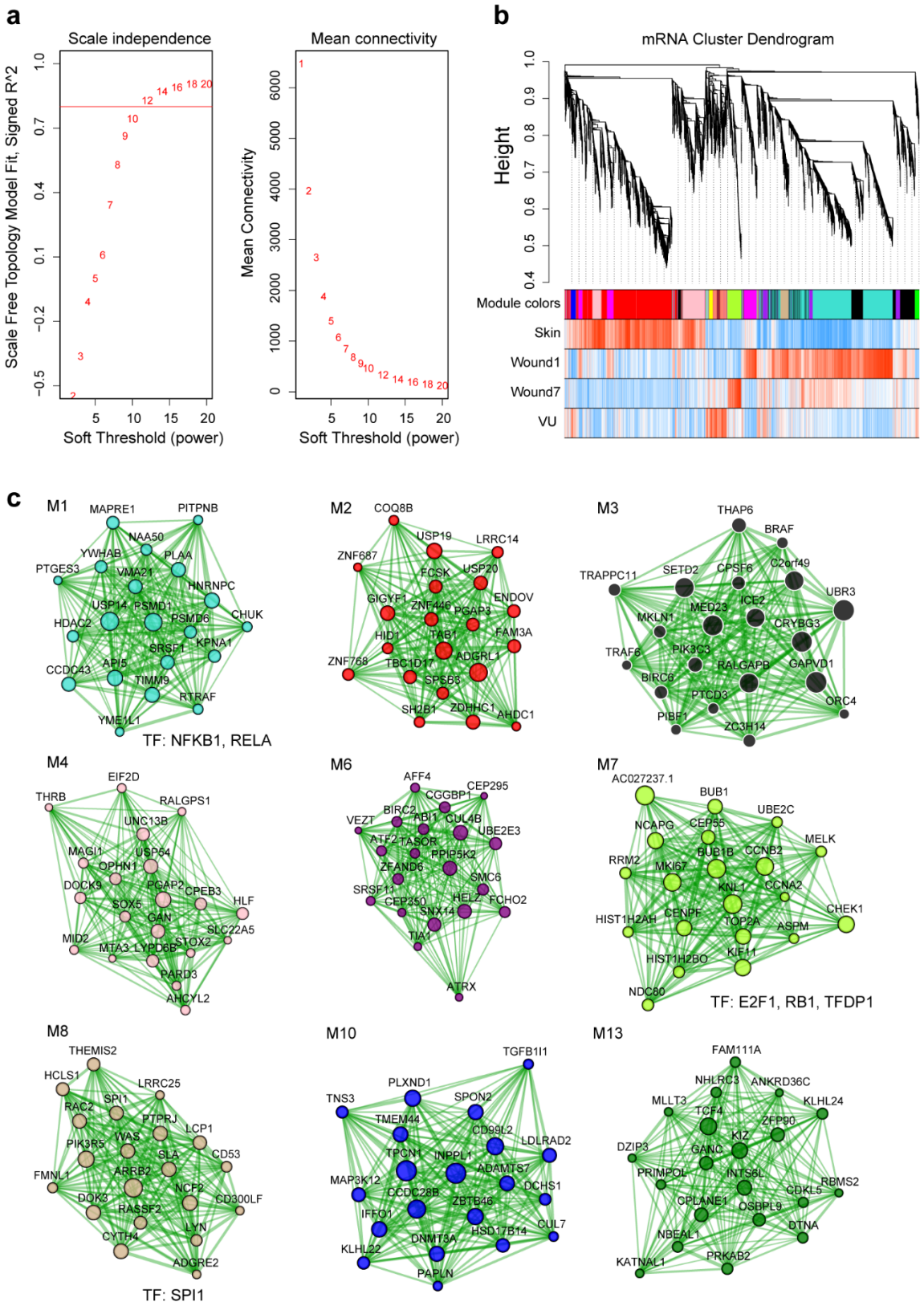

Figure 2 - figure supplement 4 Weighted gene co-expression network analysis (WGCNA) of mRNAs in human skin wound healing (related to **Figure 2e**). **a** The scale-free topology fit index (left) and mean connectivity (right) for various soft-threshold powers. The red line indicates signed R^2 = 0.8. **b** Cluster dendrogram shows mRNA co-expression modules: each branch corresponds to a module,

1033 and each leaf indicates a single miRNA. Color bars below show the module assignment (the 1st row)
1034 and Pearson correlation coefficients between mRNA expression and the sample groups (the 2nd to the
1035 5th row: red and blue lines represent positive and negative correlations, respectively). **c** Network plots
1036 of mRNA modules: the top 20 mRNAs with the highest kME values in each module were plotted in the
1037 networks. Node size and edge thickness are proportional to the kME values and the weighted
1038 correlations between two connected mRNAs, respectively. Transcription factors (TFs) with their targets
1039 enriched in the modules (Fisher's exact test: FDR < 0.05) are listed below the networks.

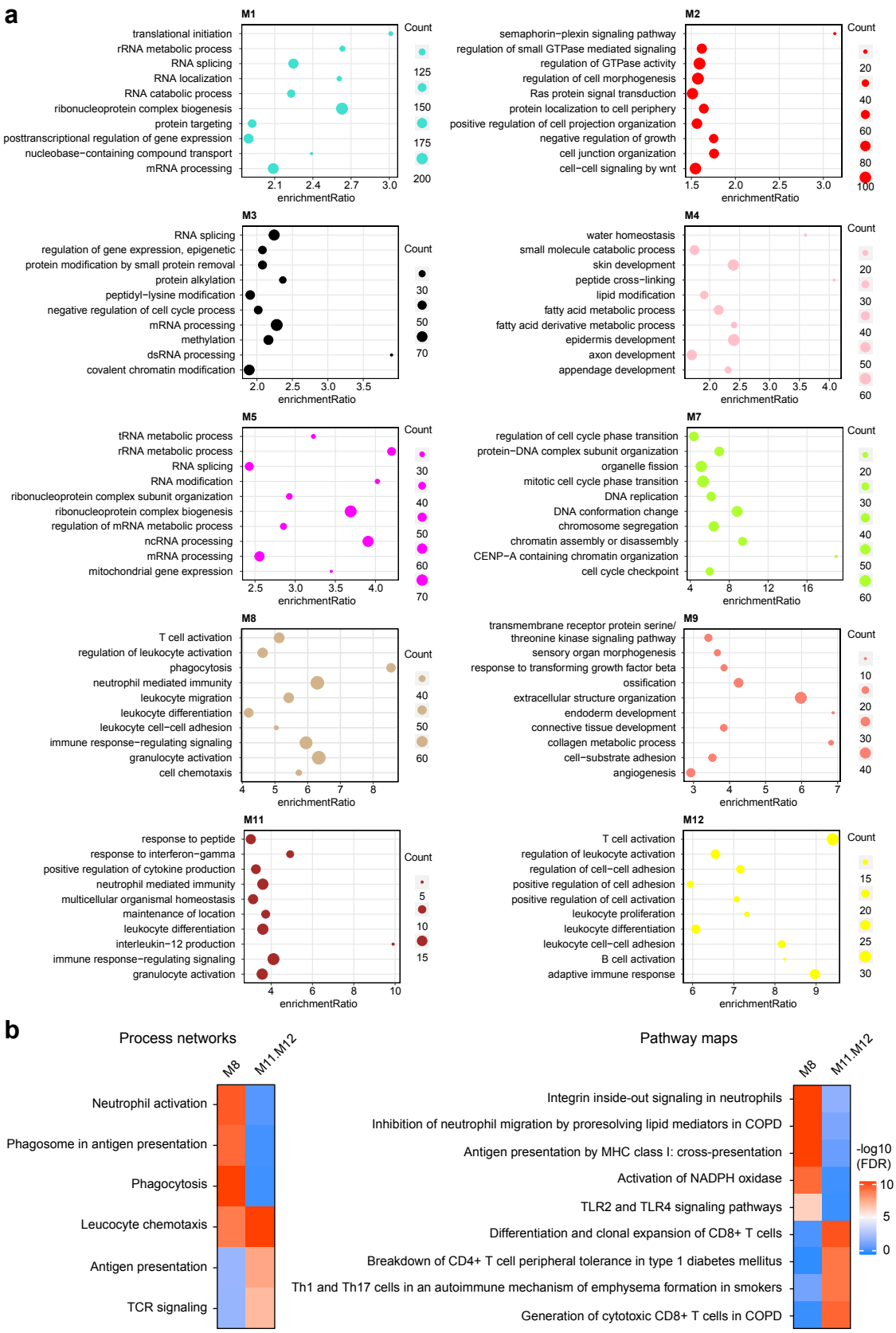

Figure 2 - figure supplement 5 Functional enrichment analysis for mRNA modules. a The top ten gene ontology (GO) terms with FDR less than 0.05 are shown for each module (related to **Figure 2f**).

1043 **b** MetaCore analysis based on a curated database identified the process networks (left) and pathway

1044 maps (right) enriched in the M8 or the combined M11.M12 modules, respectively.

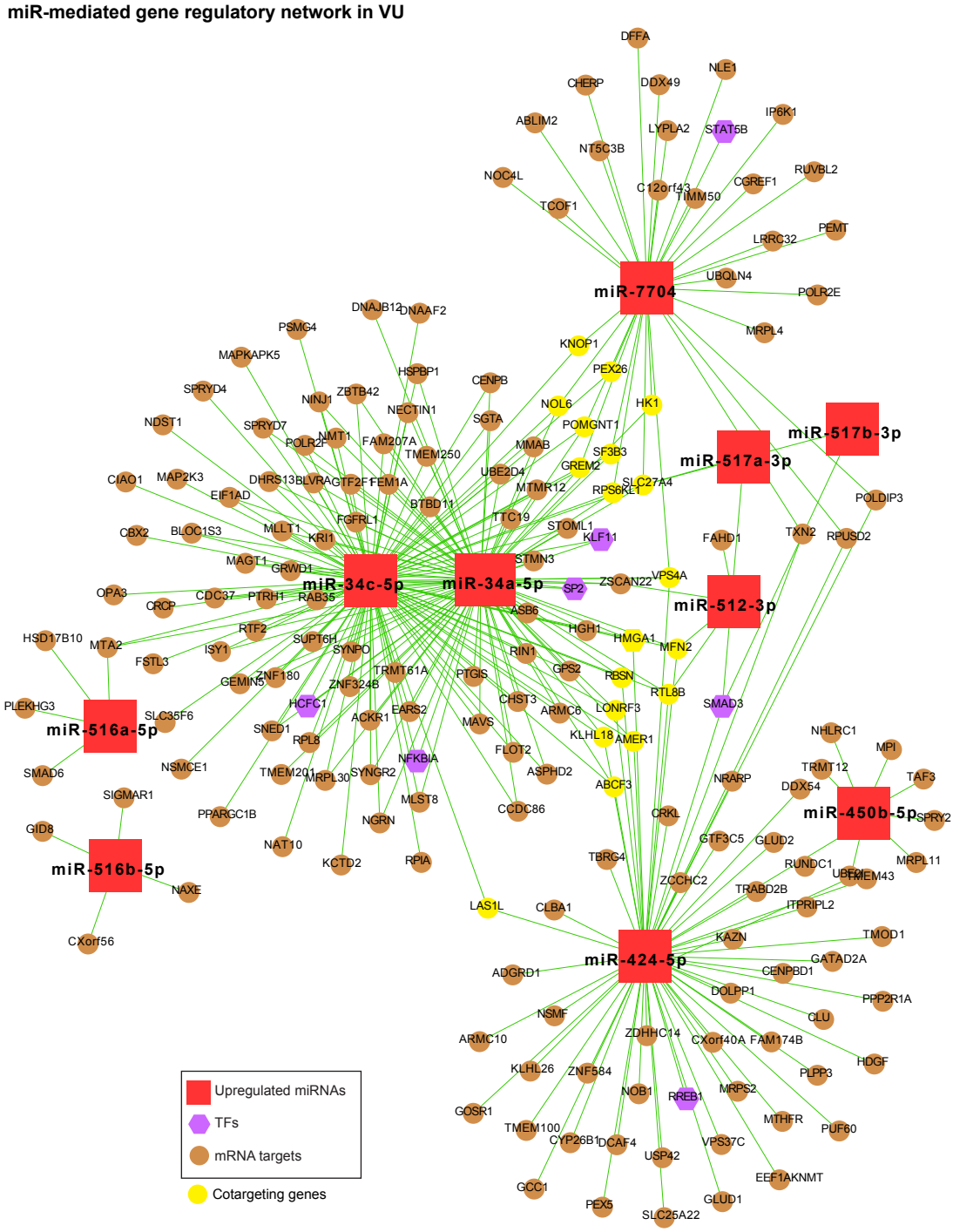

1045

1046 **Figure 4 – figure supplement 1 MiR-mediated gene regulatory network in VU**, which is constructed
1047 with the upregulated miRNAs in **Figure 4b**, the mRNAs predicted as the strongest targets and with anti-
1048 correlated expression patterns (Pearson correlation, *P-value* < 0.05 and r < 0) with these miRNAs in
1049 human wounds, and the transcription factors (TFs) regulating these miRNAs' expression from the
1050 TransmiR v2 database (related to **Figure. 4b–c** and **Additional file 8**). The mRNAs co-targeted by
1051 miRNAs with unrelated seed sequences are highlighted in yellow.

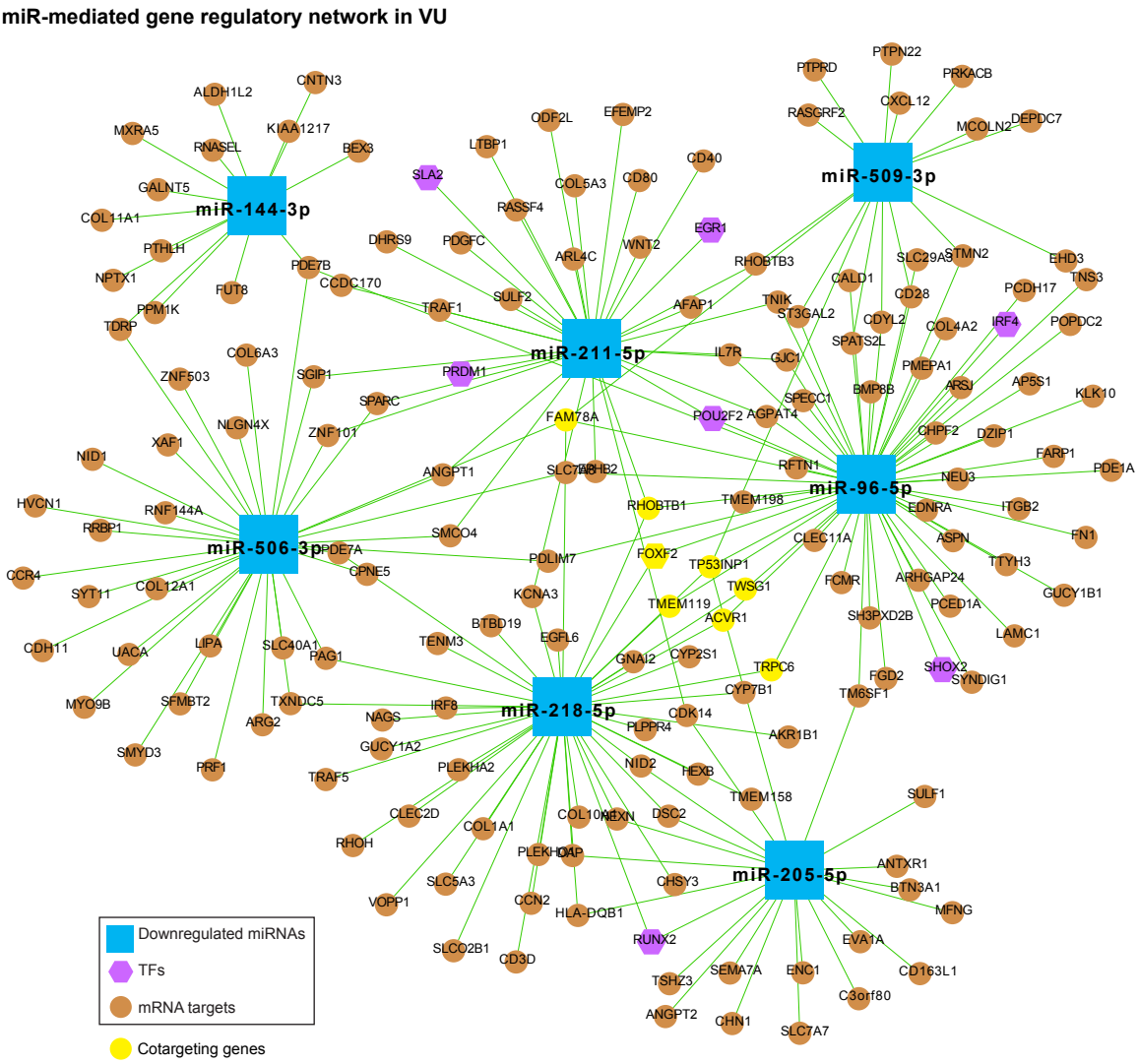

Figure 4 – figure supplement 2 MiR-mediated gene regulatory network in VU, which is constructed with the downregulated miRNAs in **Figure 4b**, the mRNAs predicted as the strongest targets and with anti-correlated expression patterns (Pearson correlation, *P-value* < 0.05 and r < 0) with these miRNAs in human wounds, and the transcription factors (TFs) regulating these miRNAs' expression from the TransmiR v2 database (related to **Figure 4b–c** and **Additional file 8**). The mRNAs co-targeted by miRNAs with unrelated seed sequences are highlighted in yellow.

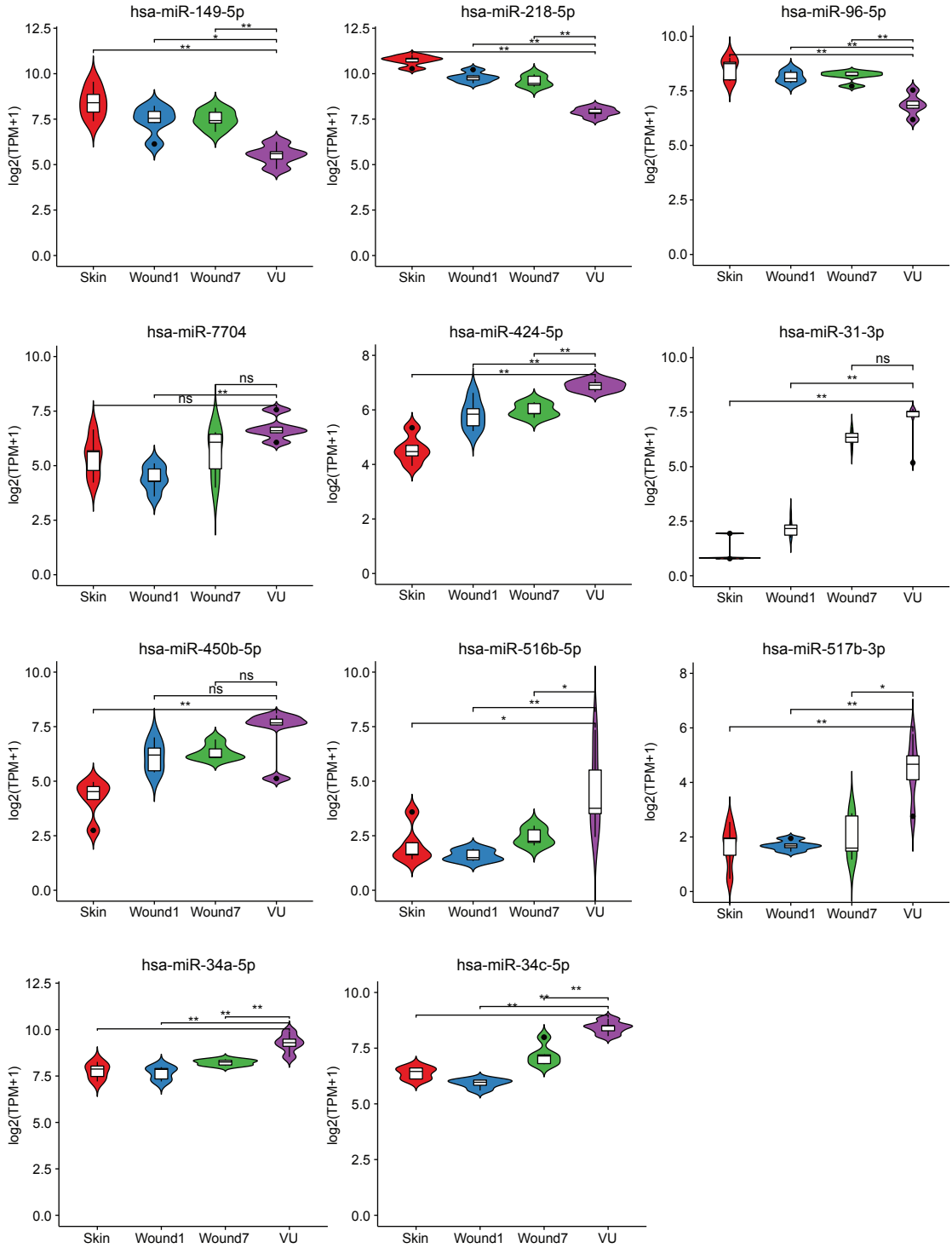

1059

1060 **Figure 5 – figure supplement 1 RNA-sequencing results for the miRNAs selected for**

1061 **experimental validation**. Mann-Whitney t-test, *P < 0.05, **P < 0.01, ns: not significant.

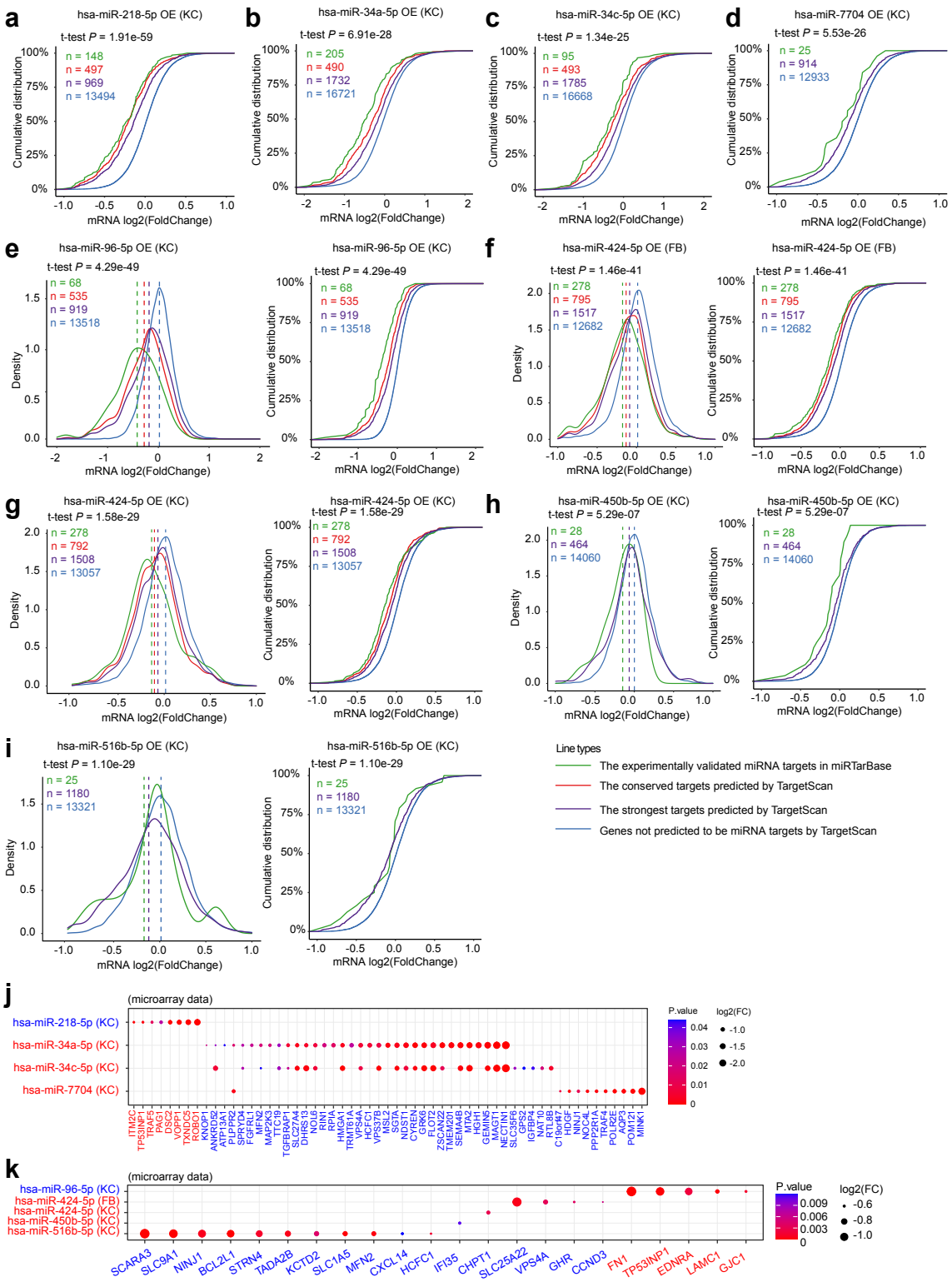

Figure 5 – figure supplement 2 Experimental validation of miRNAs' targetome. Microarray analysis was performed in keratinocytes (KC) or fibroblasts (FB) with miR-218-5p (**a**), miR-34a-5p (**b**), miR-34c-5p (**c**), miR-7704 (**d**), miR-96-5p (**e**), miR-424-5p (**f, g**), miR-450-5p (**h**), or miR-516-5p (**i**) overexpression (OE). Density plots (left) and cumulative distributions (right in **e–i**) of mRNA log2(fold

1067 change) are shown. Wilcoxon t-tests were performed to compare the TargetScan predicted strongest
1068 targets (purple) with the non-targets (blue) for each of these miRNAs. The conserved and
1069 experimentally validated targets are marked with red and green colors, respectively. Dotted lines depict
1070 the average log2(fold change) values for each mRNA group. **j, k** The target mRNAs are significantly
1071 changed (fold change < -1.2 and *P*-value < 0.05) by the indicated miRNAs in the microarray analysis.

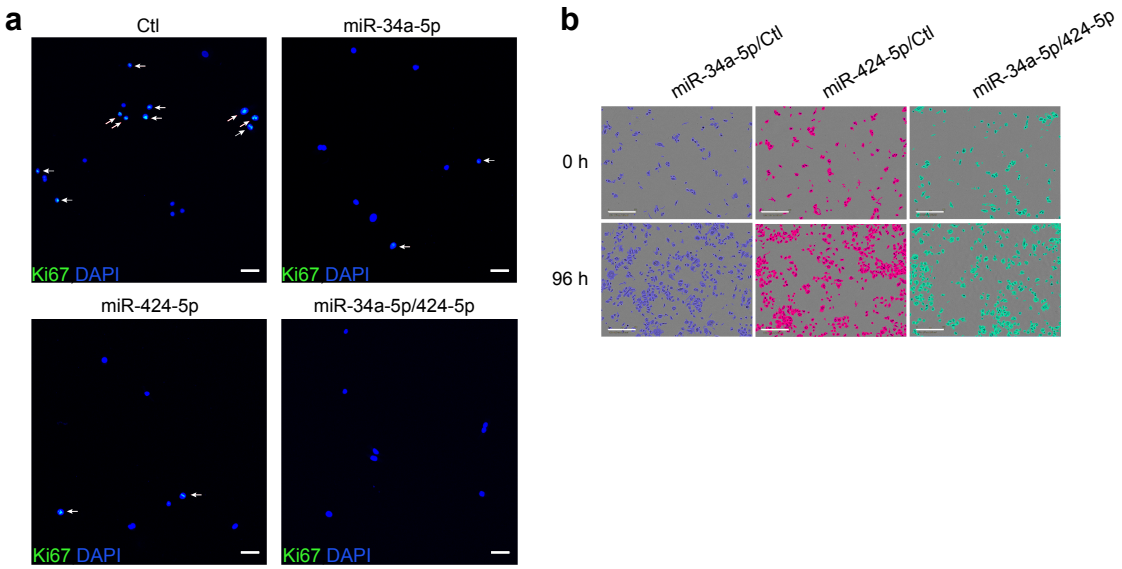

Figure 7 – supplement figure 1 Cooperation of miR-34a and miR-424 in regulating keratinocyte proliferation. **a** Ki67 expression was detected in keratinocytes transfected with miR-34a-5p or miR-424-5p mimics alone or both mimics for 24 hours by immunofluorescence staining. Cell nuclei were costained with DAPI. Ki67+ cell nuclei are highlighted with white arrows in the representative photographs. (Scale bar: 50 μm.) **b** The growth of the transfected keratinocytes (n = 3) was analyzed with a live cell imaging system, and representative photographs of cells at 0 and 96 hours are shown (Scale bar, 300 μm.).

Table 1. Characteristics of the healthy donors and the VU patients.

Characteristics	Healthy donors	Patients with VU
Study population (n)	10	12
Age, years (mean ± s.d.)	65.3 ± 3.2	75.8 ± 12.0
Ethnicity	White	White
Gender (male: female)	2:8	5:7
Biopsy location	Lower leg	Lower leg
Wound duration	Acute (1 or 7 days after injury)	3.7 ± 5.3 years

Abbreviations: s.d., standard deviation; VU, venous ulcer.

1080

1081 **Table 2. Characteristics of the patients with venous ulcer.**

Patient	Sex	Age (years)	Ethnicity	Wound size (cm)	Wound duration (years)	Wound location	Experiment
1	M	86	Caucasian	6x5	4	Lower leg	RNA-seq & qRT-PCR
2	F	68	Caucasian	15x15	2	Lower leg	RNA-seq & qRT-PCR
3	M	70	Caucasian	3x0.5	0.3	Lower leg	RNA-seq & qRT-PCR
4	F	78	Caucasian	15x12	1.5	Lower leg	RNA-seq & qRT-PCR
5	F	87	Caucasian	3x2+8x4	2.5	Lower leg	RNA-seq & qRT-PCR
6	F	73	Caucasian	3x4	3.5	Lower leg	qRT-PCR
7	M	99	Caucasian	20x10	0.5	Lower leg	qRT-PCR
8	F	71	Caucasian	20x20	20	Lower leg	qRT-PCR
9	F	77	Caucasian	2.5x3+15x15	4.5	Lower leg	qRT-PCR
10	M	51	Caucasian	2x1.5	3	Lower leg	qRT-PCR
11	M	69	Caucasian	12x15	1	Lower leg	qRT-PCR
12	F	81	Caucasian	7x2.5	1	Lower leg	qRT-PCR

1082 Abbreviations: M, male; F, female.

1083 **Table 3. Characteristics of the healthy donors.**

Donor	Sex	Age (years)	Ethnicity	Wound location	Experiment
1	F	66	Caucasian	Lower leg	RNA-seq
2	M	69	Caucasian	Lower leg	RNA-seq
3	F	67	Caucasian	Lower leg	RNA-seq
4	M	69	Caucasian	Lower leg	RNA-seq & qRT-PCR
5	F	64	Caucasian	Lower leg	RNA-seq & qRT-PCR
6	F	60	Caucasian	Lower leg	qRT-PCR
7	F	66	Caucasian	Lower leg	qRT-PCR
8	F	60	Caucasian	Lower leg	qRT-PCR
9	F	67	Caucasian	Lower leg	qRT-PCR
10	F	65	Caucasian	Lower leg	qRT-PCR

1084 Abbreviations: M, male; F, female.

1085 **Video 1**. **Keratinocyte growth was analyzed with a live cell imaging system.** 1, Keratinocytes co-
1086 transfected with miR-34a-5p and control mimics. 2, Keratinocytes co-transfected with miR-424-5p and
1087 control mimics. 3, Keratinocytes co-transfected with miR-34a-5p and miR-424-5p mimics.
1088
1089 **Additional file 1.** Source data for miRNAs (related to **Figure 1c, d**) and mRNA (related to **Figure 1e**)
1090 with expression change specifically in venous ulcers.
1091
1092 **Additional file 2.** Source data for weighted gene co-expression network analysis of miRNAs in wound
1093 healing. (related to **Figure 2a, b**)
1094
1095 **Additional file 3.** Source data for the top 20 driver miRNAs of each significant module in WGCNA.
1096 (related to **Figure 2c, d** and **Figure supplements 2-2**)
1097
1098 **Additional file 4.** Source data for transcription factors (TF) regulating miRNA expression in each
1099 module. (related to **Figure 2c, d** and **Figure supplements 2-2b-2i**)
1100
1101 **Additional file 5.** Source data for weighted gene co-expression network analysis of mRNAs in wound
1102 healing. (related to **Figure 2e**)
1103
1104 **Additional file 6**. Source data for transcription factors (TF) with targets enriched in significant mRNA
1105 modules. (related to **Figure supplements 2-4c**)
1106
1107 **Additional file 7.** Source data for gene set enrichment analysis for VU-affected DE mRNAs and mRNA
1108 modules in the strongest targets of VU-associated DE miRNAs and miRNA modules. (related to **Figure**
1109 **4a**)
1110
1111 **Additional file 8.** Source data for the individual candidate miRNAs with their targets enriched for the
1112 VU mRNA signature. (related to **Figure 4b**)
1113
1114 **Additional file 9.** Source data for experimental validation of miRNAs' expression in human skin wounds
1115 (related to **Figure 5a-i**), enrichment analysis of the experimentally validated miRNA targets for the
1116 venous ulcer (VU) gene signature (related to **Figure 5n**), and miRNA targets validated by the microarray
1117 and in VU gene signature (related to **Figure supplements 5-2j, 2k**).
1118
1119 **Additional file 10.** Source data for gene ontology analysis of the miRNA-regulated genes in the
1120 microarray data. (related to **Figure 6**)
1121
1122 **Additional file 11.** Source data for cooperation of miR-34a, miR-424, and miR-516 in regulating
1123 keratinocyte proliferation and inflammatory response. (related to **Figure 7b-e**)
1124

1125 **Table S1.** Quality control of small RNA sequencing data.
1126
1127 **Table S2.** Quality control of rRNA-depleted total RNA sequencing data.